Supporting Information

Benchmark Study of Hydrogen Storage in Metal–Organic Frameworks under Temperature and Pressure Swing Conditions

Paula García-Holley,[a] Benjamin Schweitzer,[b] Timur Islamoglu,[a] Yangyang Liu,[a] Lu Lin,[a] Stephanie Rodriguez,[c] Mitchell Weston,[c] Joseph T. Hupp,[a] Diego A. Gómez-Gualdrón,*[c] Taner Yildirim*[d] and Omar K. Farha*[a,e]

[a] Department of Chemistry, Northwestern University, Evanston, IL 80202, USA

[b] Department of Chemical and Biological Engineering, Colorado School of Mines, Golden, CO 80401, USA

[c] NuMat, Skokie, IL 60077, USA

[d] NIST center for Neutron Research, National Institute of Standards and Technology, Gaithersburg, MD 20899, USA

[e] Department of Chemistry, Faculty of Sciences, King Abdulaziz University, Jeddah 21589, Saudi Arabia.

Table of Contents **Page**

Section S1. Materials
All chemicals and solvents were purchased from Aldrich (Milwaukee, WI) and used without further purification with exception of bis(pinacolato)diboron which was purchased from Combi-Blocks (San Diego, CA). Deionized water used was provided by Northwestern University. Deuterated solvents were purchased from Cambridge Isotope Laboratories (Andover, MA).
Gases used were ultra high purity grade 5 and were purchased from Airgas Specialty Gases (Chicago, IL).

Section S2. Instrumentation
^{1}H NMR spectra were obtained in a Bruker AVANCE III 500 MHz spectrometer.
Supercritical CO_2 drying of the MOFs (when indicated) was performed with a Tousimis™ Samdri® PVT-30 critical point dryer by Tousimis (Rockville, MD).
N_2 isotherms at Northwestern University were performed with a Micromeritics (Norcross, GA) Tristar II at 77 K (held constant by a liquid N_2 bath).
N_2 Isotherms and Excess and total H_2 uptake were measured at NIST on a computer-controlled Sieverts instrument.[1]
PXRD patterns were obtained from a Rigaku Smartlab® with a high intensity Cu rotating anode generator.

Section S3. Experimental Methods
MOF samples NU-125,[2] PCN-250,[3] Zn_2(1,4-bdc)$_2$(dabco),[4] HKUST-1,[5] NU-1000,[6,7] UiO-67,[8] were synthesized using previously published procedures.

NOTT-112 ligand, 1,3,5-Tris(3',5'-dicarboxy[1,1'-biphenyl]-4-yl-)benzene (H_6TDBB)

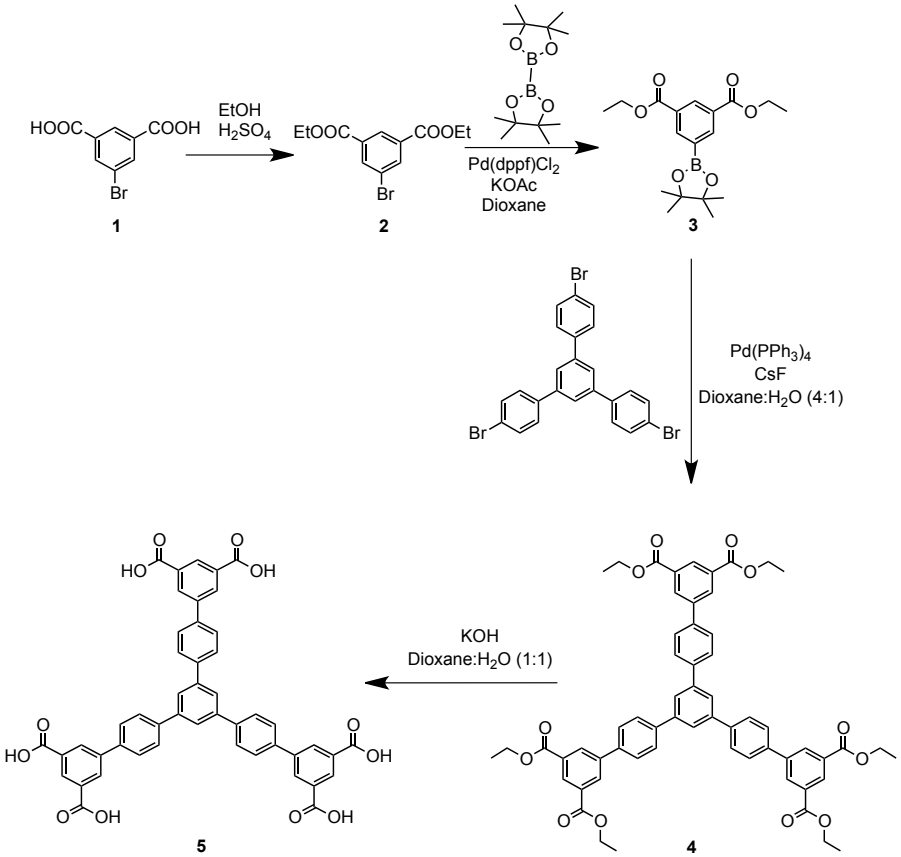

Scheme S1. Synthesis of 1,3,5-tris(3',5'-dicarboxy[1,1'-biphenyl]-4-yl-)benzene (H_6TDBB)

Synthesis of **2**:
5-bromideisophthalate (5.00 g, 20.4 mmol) was dissolved in 50 mL of EtOH and five drops of conc. H_2SO_4. The solution was heated to reflux with constant stirring for 24 h. The reaction mixture was concentrated using rotary evaporation, and the product was suspended in H_2O and extracted with ethyl acetate followed by washing with bicarbonate rinses. The ethyl acetate was removed under vacuum and the product was recrystallized from pentane.

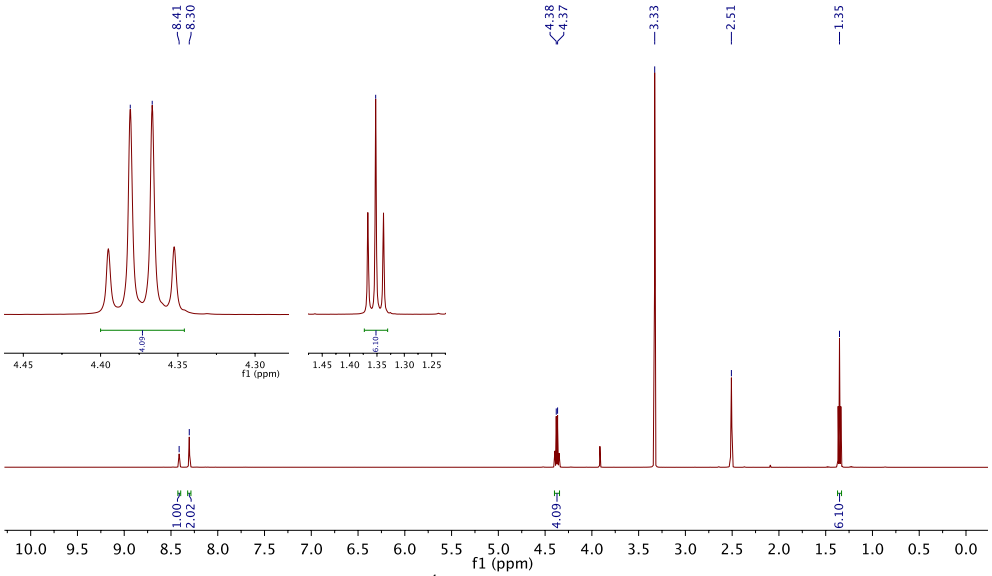

Figure S1. ^{1}H NMR spectrum of **2**

Synthesis of **3**:
Compound **2** (5.00 g, 16.6 mmol), $Pd(dppf)Cl_2$ (0.304 g, 4.15 mmol), bis(pinacolato)diboron (4.64 g, 18.3 mmol) and KOAc (4.88 g, 49.7 mmol) was added to a 250-mL round bottom flask. 100 mL of 1,4-dioxane was added and the mixture was purged with Ar and the flask was sealed and heated with stirring at 90 ºC for 24 h. The product was purified using a silica gel column with 5% v/v ethyl acetate in hexane.

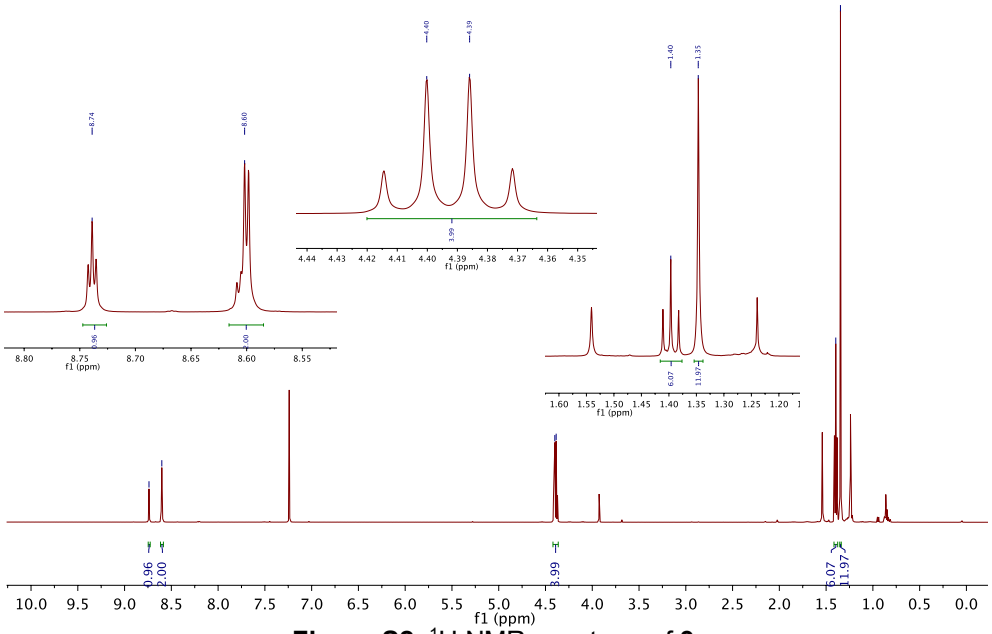

Figure S2. ^{1}H NMR spectrum of **3**

Synthesis of **4**:
Compound **3** (5.00 g, 14.4), 4,4''-dibromo-5'-(4-bromophenyl)-1,1':3',1''-terphenyl (2.36 g, 4.35 mmol), CsF (6.61 g, 43.5 mmol), and $Pd(PPh_3)_4$ (2.51 g, 2.17 mmol) was added to 100 mL of an Ar purged mixture of 1,4-dioxane:H_2O (4:1 by volume). The reaction mixture was heated in a capped container under argon at 90 ºC for 24 h. The product was dissolved in dichloromethane and the impurities were extracted with H_2O and the organic layer was dried with $MgSO_4$. The product was purified using a silica gel column with 1% v/v ethyl acetate in dichloromethane solution.

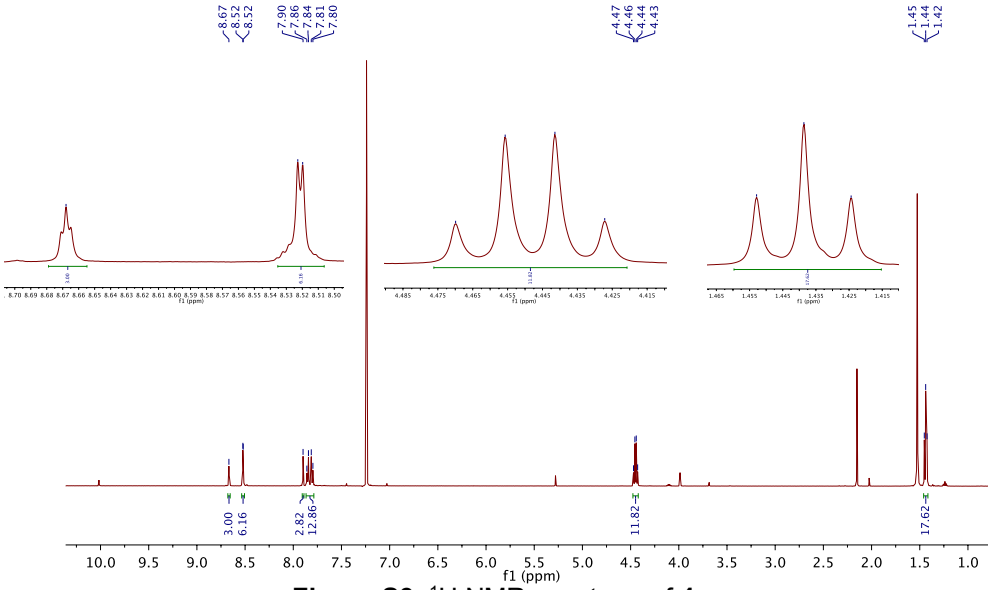

Figure S3. ^{1}H NMR spectrum of **4**

Synthesis of **5**:
Compound **4** (1.50 g, 1.55 mmol) was dissolved in 100 mL of a 1,4-dioxane:H_2O (1:1) mixture to which 1.5 g (26.7 mmol) of KOH were added. The reaction mixture was heated under reflux with stirring for 48 h and then the solvent was removed under vacuum. The product was dissolved in 400 mL of H_2O and concentrated HCl was added until a pH of 1 was reached. The product was filtered and washed with H_2O and methanol.

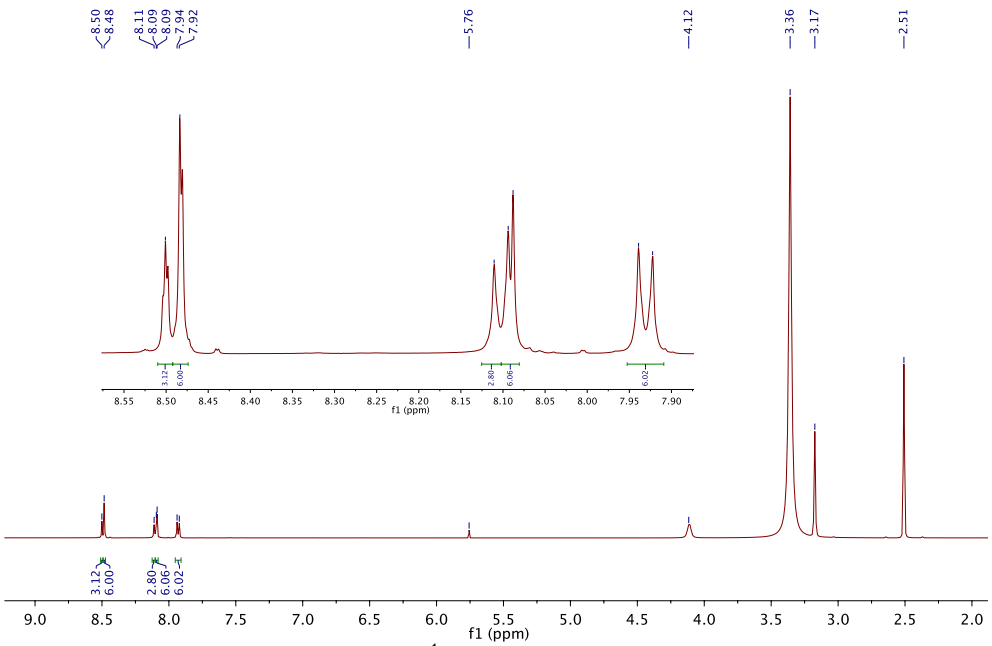

Figure S4. ^{1}H NMR spectrum of **5**

NOTT-112:

NOTT-112 was synthesized using a modified NU-125 procedure.[2] DMF (10 mL) was added to a mixture of 43.3 mg (0.054 mmol) of H_6TDBB and 100 mg (0.43 mmol) of $Cu(NO_3)_2 \cdot 2.5H_2O$ in an 8-dram vial. Five drops of HBF_4 was added and the solution was heated at 80 ºC for 24 h.

The product was then washed three times with DMF (once every two hours) and left overnight soaking in ethanol after and later washed two more times with ethanol (once every two hours). Ethanol was removed via supercritical CO_2 supercritical drying after which all handling of the material was done in an Ar-filled glovebox.

UiO-68-Ant:

To a mixture of $ZrCl_4$ (23.3 mg, 0.100 mmol) and 9,10-anthacenyl bis(benzoic acid) (42.0 mg, 0.100 mmol) in a 2.0 dr vial with DMF (3 mL) add 600 µL of conc. acetic acid. After sonication heat in oven at 120 ºC for 24 h. A procedure for this ligand was previously reported.[9]

The product was then washed three times with DMF (once every two hours) and left overnight soaking in acetone after and later washed two more times with acetone (once every two hours). The MOF was dried in a vacuum oven and then activated at 110 ºC for 12 h.

MOF-74-Cu

2,5-dihydroxyterephthalic acid (4.66 g, 23.5 mmol) and copper nitrate (II) trihydrate (12.6 g, 52.5 mmol) were dissolved in 525 mL of 20:1 (v/v) solution of *N*,*N*-dimethylformamide (DMF) and 2-propanol in a 1 L screw cap bottle. The suspension was sonicated for approximately 10 minutes until a homogenous solution was achieved and then degassed by bubbling nitrogen through the solution for approximately 5 minutes. The solution was placed in an oven at 80 ˚C for 18 h. After, the sample was cooled down to room temperature and the supernatant solution was decanted. The reddish needle-shaped crystals were washed with DMF and solvent exchanged with methanol 4 times over a 48 h period. The sample was activated at 150 ˚C to yield MOF-74-Cu ($Cu_2(C_8H_2O_6)$).

CYCU-3-Al

Firstly, $AlCl_3 \cdot 9H_2O$ (0.53 g, 1.98 mmol) was dissolved in 10 mL of DMF (10 mL). Then CF_3COOH (0.12 mL) and 4,40-stilbenedicarboxylic acid (H_2SDC) (1.073 g, 4 mmol) and TFA (0.12 mL) were added to the solution. After sonicating for 5 min, the mixture was heated in an oven at 140 ºC for 48 h. The solid was separated by centrifugation and washed with fresh DMF and acetone for three times, respectively. The sample was later activated at 100 °C under vacuum for 24 h.[10]

rht-MOF-7 ligand, 2,4,6-tris(3,5-dicarboxylphenylamino)-1,3,5-triazine (H_6TDPAT)

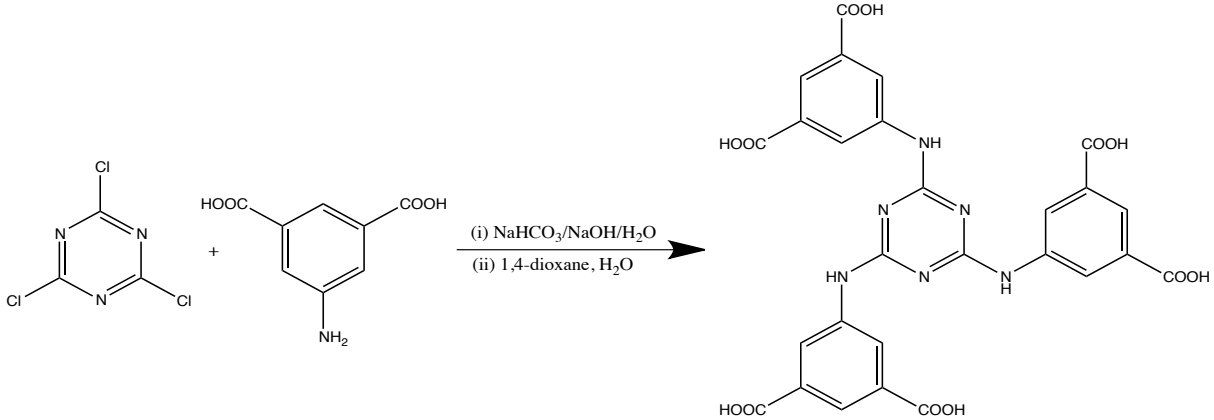

Scheme S2. Synthesis of 2,4,6-tris(3,5-dicarboxylphenylamino)-1,3,5-triazine (H_6TDPAT)

The ligand was prepared using a literature procedure with minor modifications.[11] 5-aminoisophthalate (15.2 g), KOH (7.5183 g) and $NaHCO_3$ were placed in a 500-mL round bottom flask and placed in an ice bath. H_2O (140 mL) was added and the reaction mixture was stirred for 30 min at 0 ºC. Additionally, a solution of cyanuric chloride (3.68 g) in 1,4-dioxane (70 mL) was added dropwise to the aqueous reaction mixture while still in the ice bath. Once addition of cyanuric chloride was completed, the reaction was heated to 100 ºC with stirring for

24 h. HCl was added to the resulting solution until a pH of 2 was reached at which point the product precipitated out. The product was filtered and washed with H_2O.

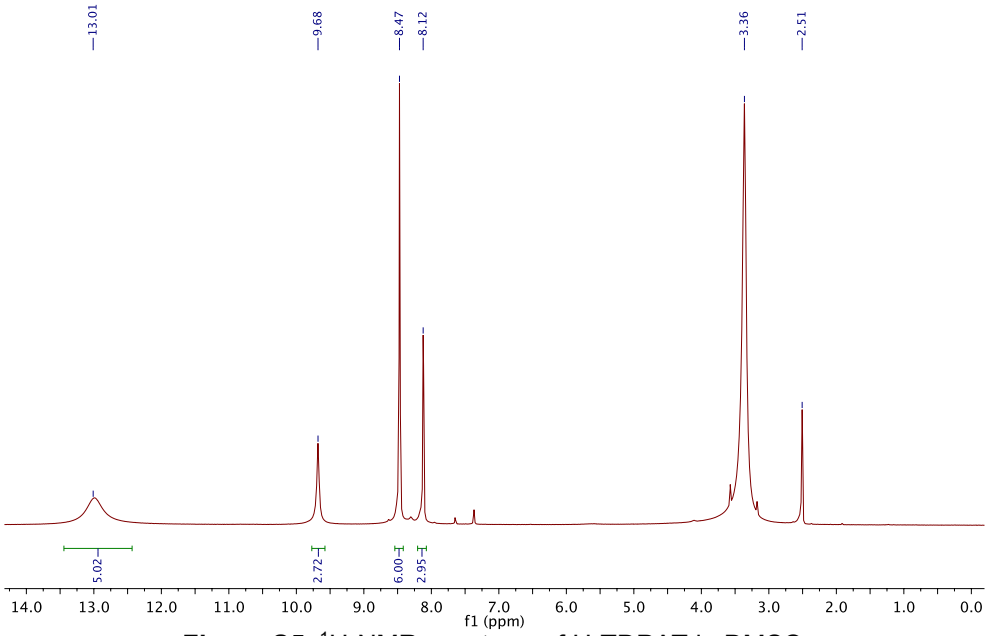

Figure S5. ^{1}H-NMR spectrum of H_6TDPAT in DMSO

rht-MOF-7

rht-MOF-7 was synthesized using a combination of modified literature procedures.[2, 12] A solution of H_6TDPAT (0.0322 g) in DMF (10 mL) was heated at 100 ºC for an hour until it was fully dissolved. $Cu(NO_3)_2 \cdot 2.5H_2O$ (100 mg) was added to the reaction mixture after which it was heated in an oven at 65 ºC for 5 days. The product was washed and activated following the same conditions as NOTT-112.

Section S4. Computational Methods

Intermolecular interactions were described according to the potentials illustrated below. A Lennard-Jones (LJ) plus Coulomb potential was used to describe interactions involving nitrogen molecules, whereas a similar potential but introducing quantum (Feymann-Hibbs) corrections were used to describe interaction involving hydrogen molecules.

Lennard-Jones (LJ) + Coulomb potential

$$V_{ij} = 4\varepsilon_{ij}\left[\left(\frac{\sigma_{ij}}{r_{ij}}\right)^{12} - \left(\frac{\sigma_{ij}}{r_{ij}}\right)^{6}\right] + \frac{q_i q_j}{4\pi\epsilon_o r_{ij}}$$

Feymann-Hibbs correction to Lennard-Jones + Coulomb potential

$$V_{ij} = \frac{4\varepsilon_{ij}}{{r_{ij}}^2}\frac{\hbar^2}{24\mu_{ij}k_B T}\left[132\left(\frac{\sigma_{ij}}{r_{ij}}\right)^{12} - 30\left(\frac{\sigma_{ij}}{r_{ij}}\right)^{6}\right] + \frac{q_i q_j}{4\pi\epsilon_o r_{ij}}$$

The sites used to describe the nitrogen and hydrogen molecules are shown below, and the corresponding parameters of the sites are shown in Table S1. Parameters for MOF sites are shown in Table S2.

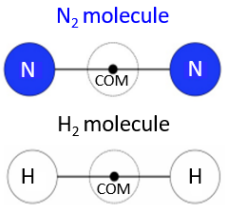

Table S1. Force field parameters for hydrogen and nitrogen molecules

Site	ε [K]	σ [Å]	q (e)
H@H_2	0.00	0.000	+0.468
com@H_2	36.7	2.958	-0.936
N@N_2	36.0	3.310	-0.462
com@N_2	0.00	0.000	+0.964

Table S2: Lennard Jones parameter for MOF atoms.

Site	ε [K]	σ [Å]
Al	254.336	3.964
C	52.882	3.431
Cu	2.518	3.114
Fe	6.547	2.594
H	22.160	2.571
N	34.751	3.266
O	30.218	3.118
Zn	62.451	2.462
Zr	34.751	2.783

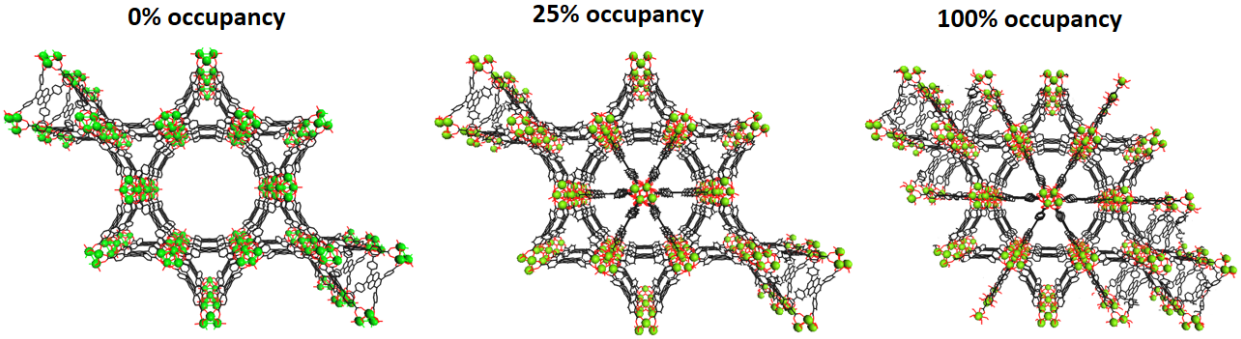

Figure S6. *In silico* models for NU-1000 differing in the "occupancy" of the hexagonal channels. Perfect NU-1000 (0% occupancy) presents the **csq** topology. The completely imperfect NU-1000 (100% occupancy) presents the **shp** topology. Partially imperfect NU-1000 (25% occupancy) is consistent with experimental measurements.

Section S5. Powder XRD Patterns

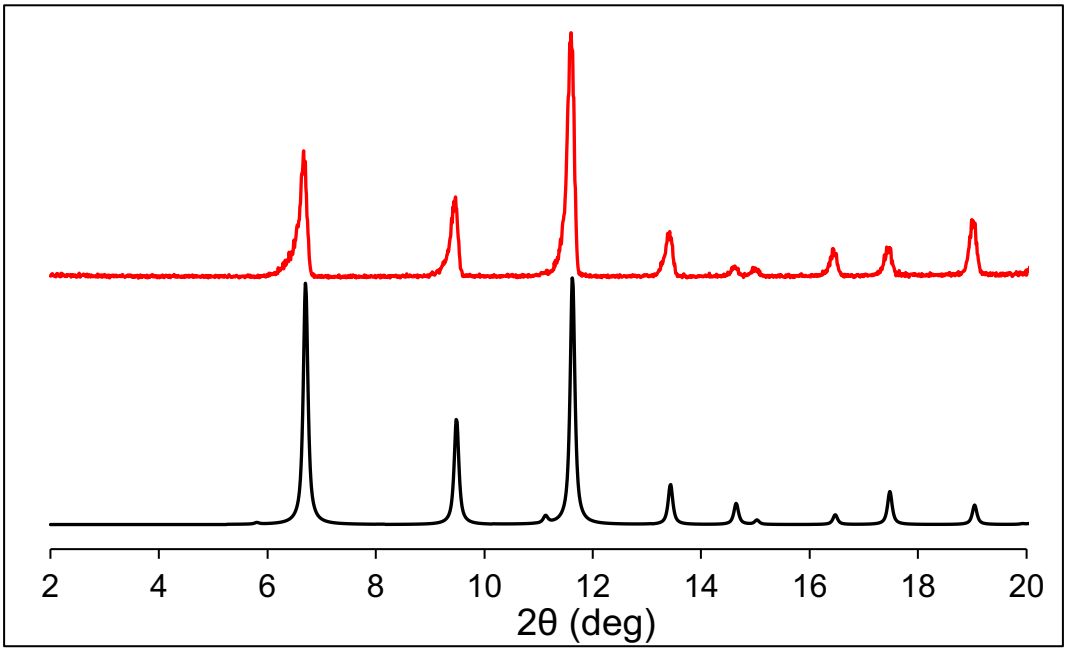

Figure S7. Simulated (black) and experimental (red) PXRD patterns for HKUST-1

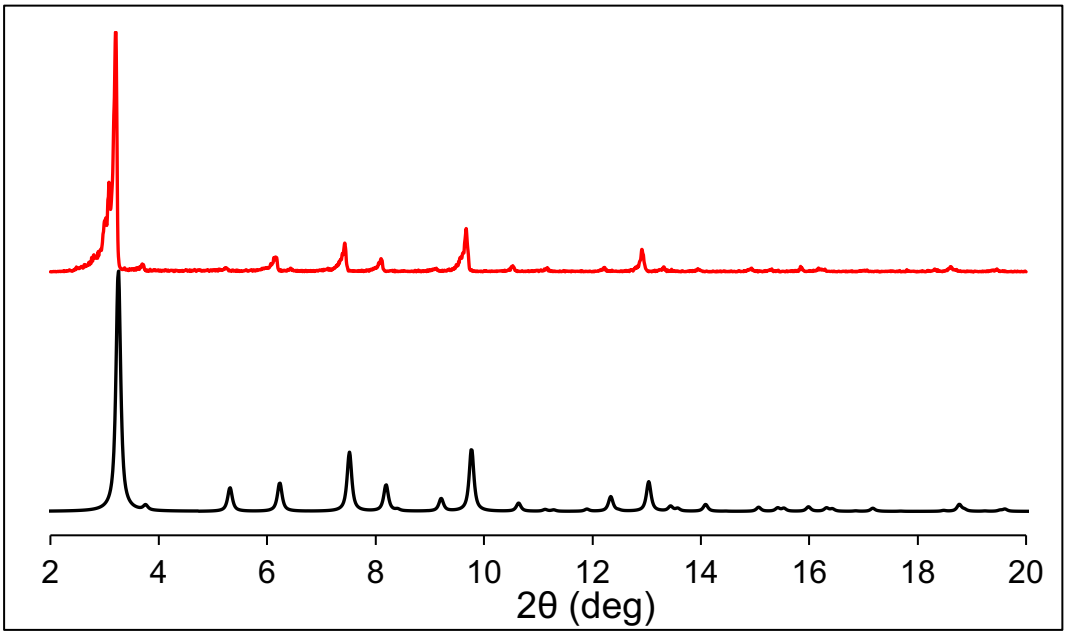

Figure S8. Simulated (black) and experimental (red) PXRD patterns for NOTT-112

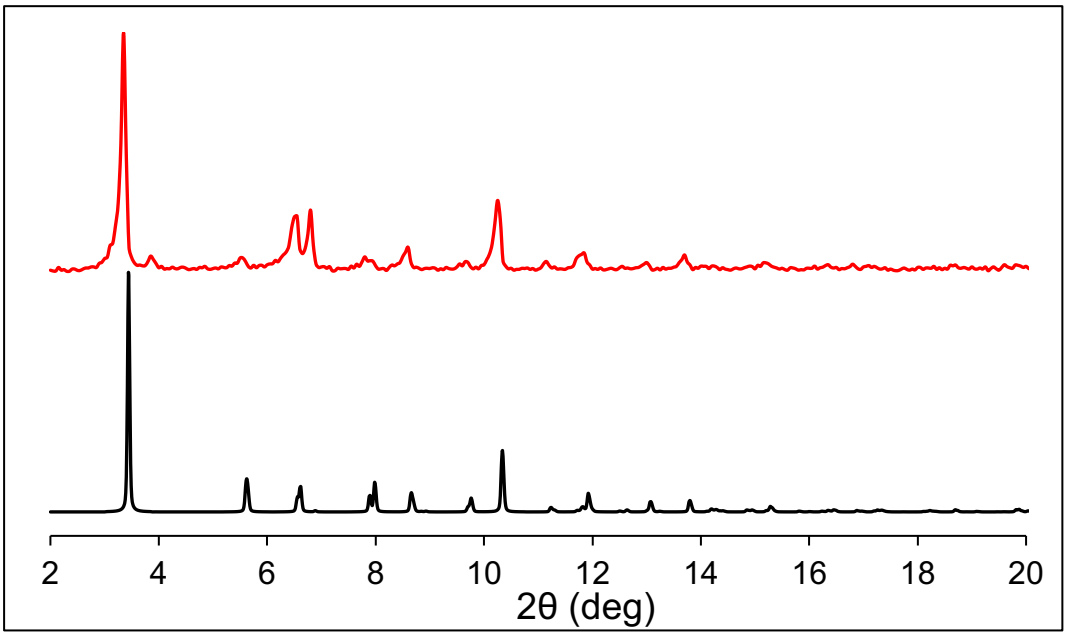

Figure S9. Simulated (black) and experimental (red) PXRD patterns for NU-125

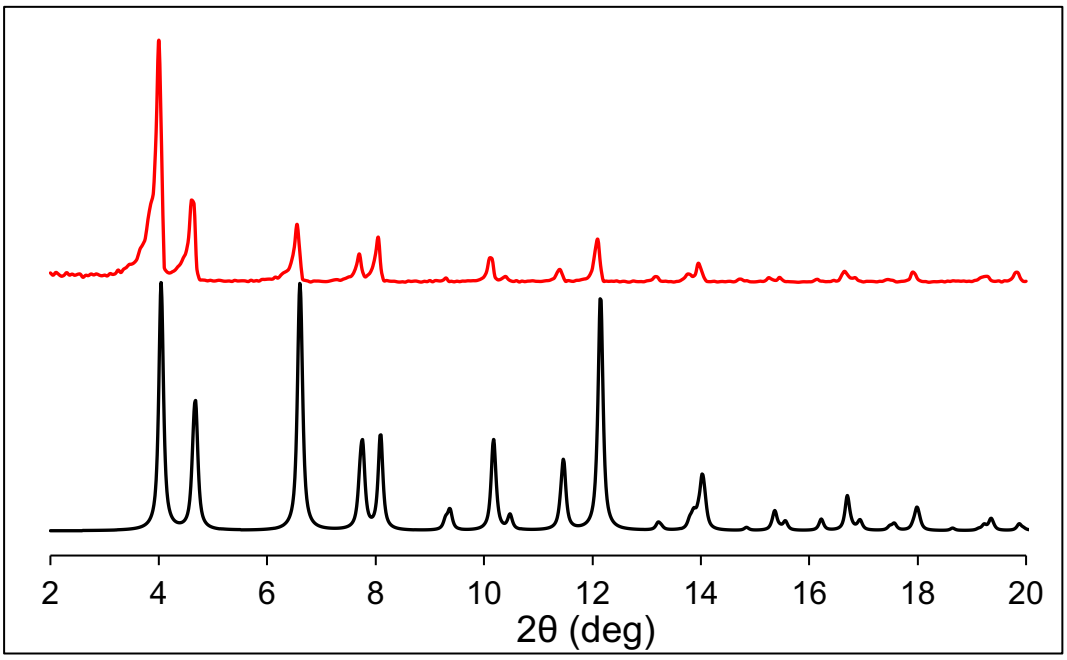

Figure S10. Simulated (black) and experimental (red) PXRD patterns for rht-MOF-7

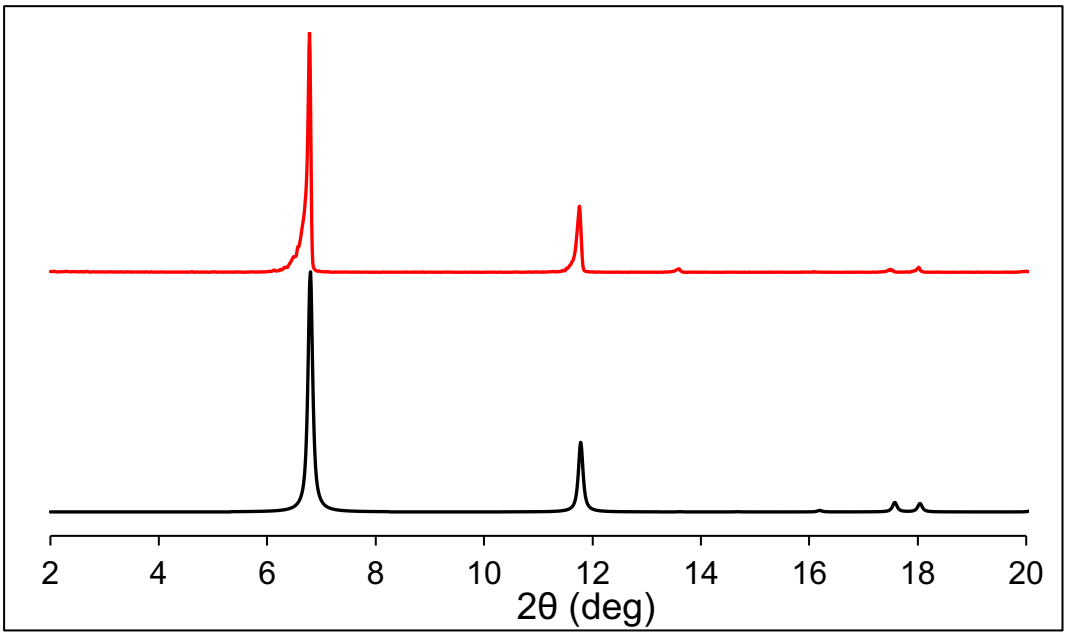

Figure S11. Simulated (black) and experimental (red) PXRD patterns for Cu-MOF-74

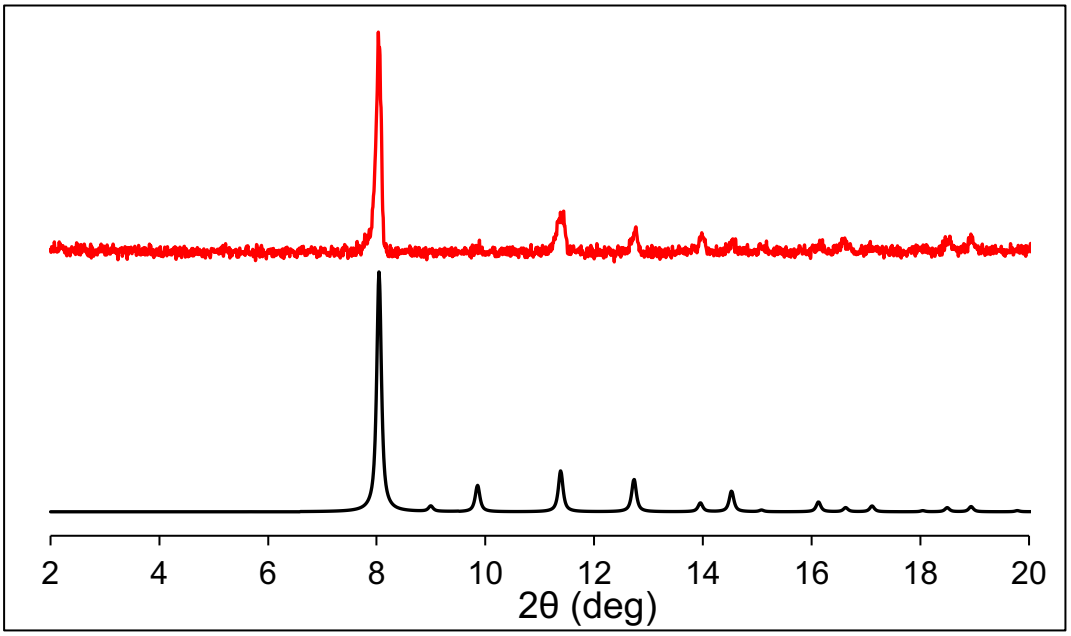

Figure S12. Simulated (black) and experimental (red) PXRD patterns for PCN-250

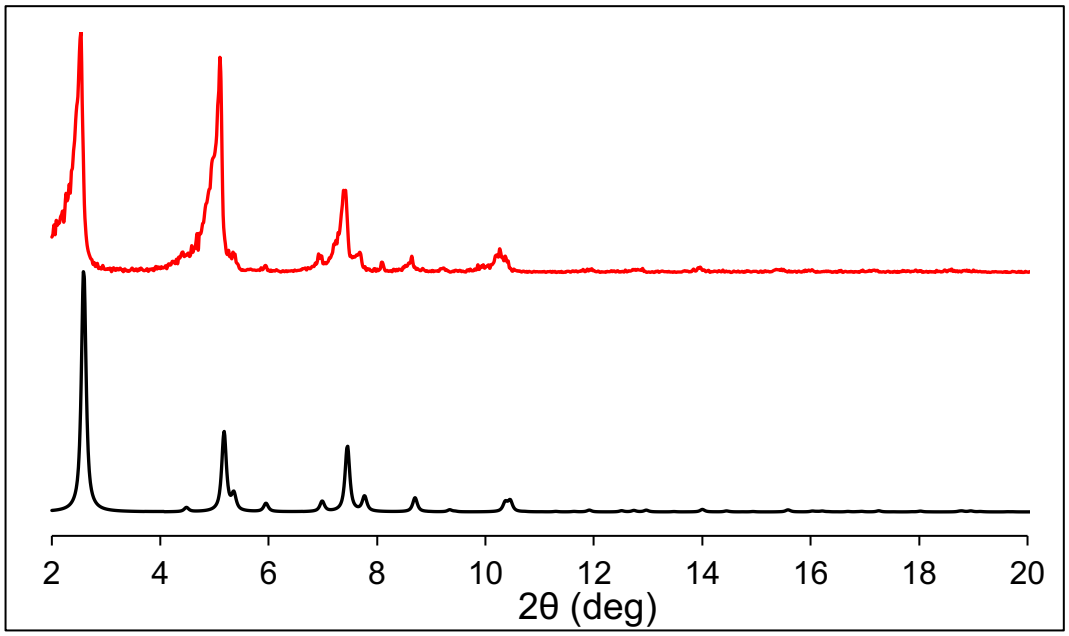

Figure S13. Simulated (black) and experimental (red) PXRD patterns for NU-1000

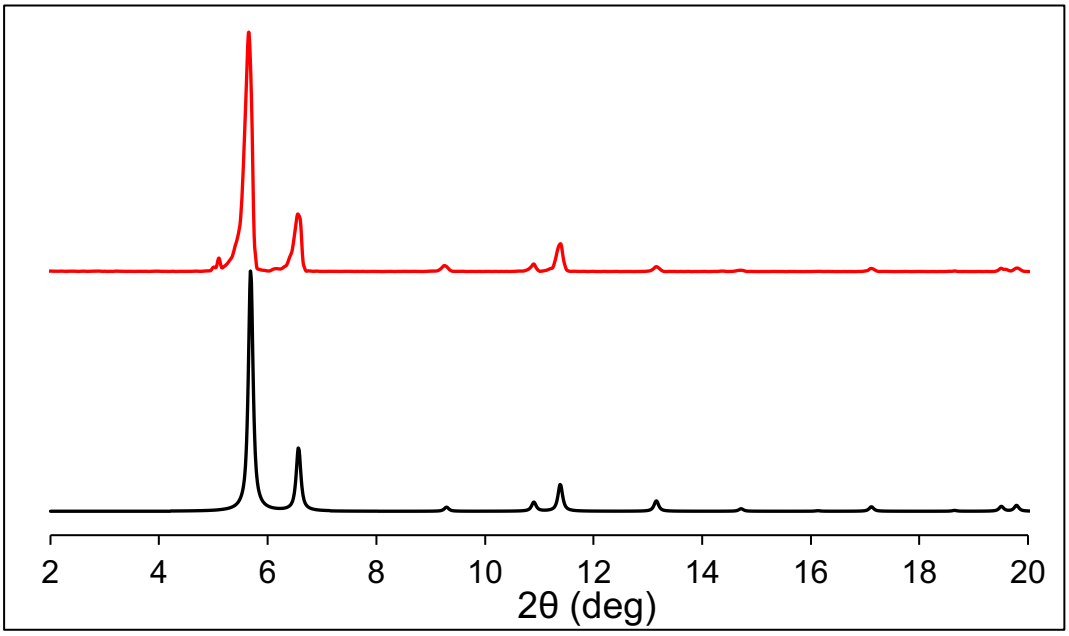

Figure S14. Simulated (black) and experimental (red) PXRD patterns for UiO-67

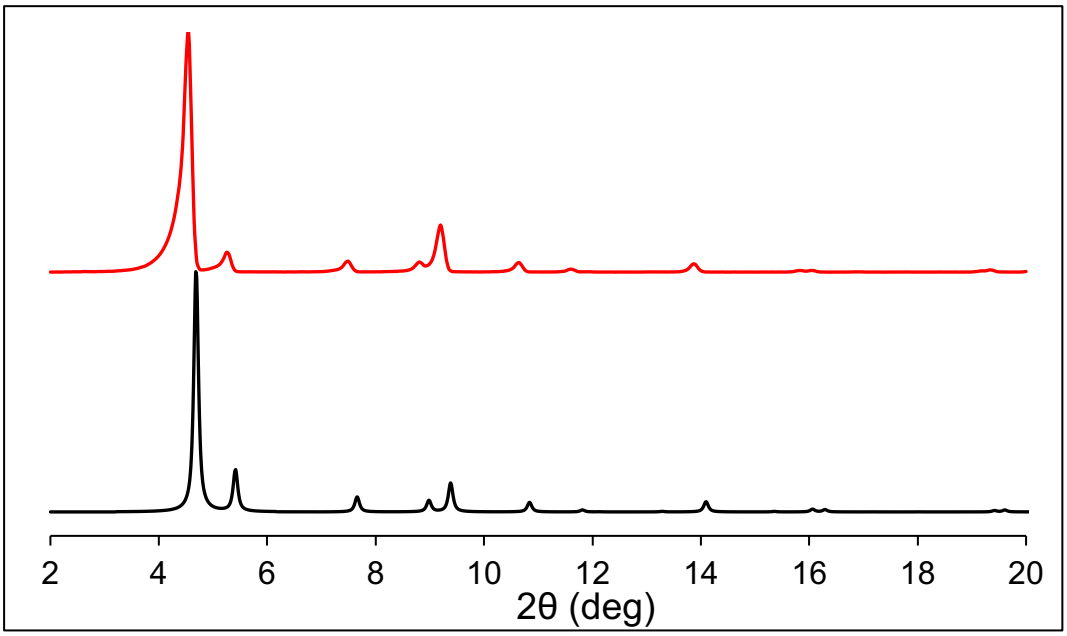

Figure S15. Simulated (black) and experimental (red) PXRD patterns for UiO-68-Ant

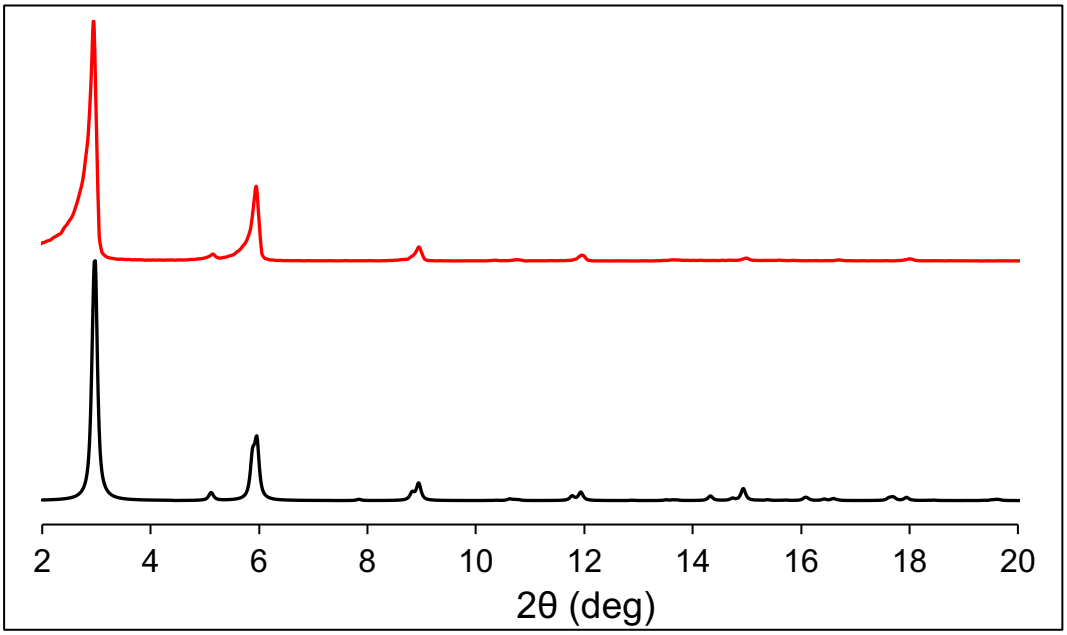

Figure S16. Simulated (black) and experimental (red) PXRD patterns for CYCU-3-Al

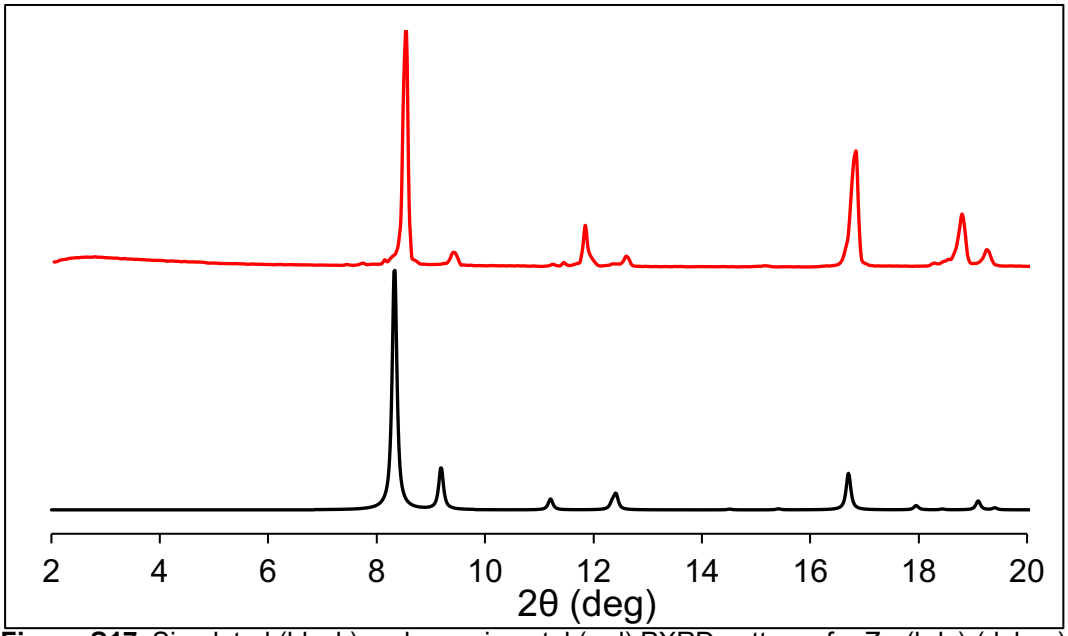

Figure S17. Simulated (black) and experimental (red) PXRD patterns for $Zn_2(bdc)_2(dabco)$

Section S6. Nitrogen Isotherm Data

Brunauer–Emmett–Teller (BET) areas were determined by applying the BET model to the nitrogen isotherms, ensuring that the four consistency criteria are met.[13] Pore volumes were calculated from the nitrogen saturation loadings.

Table S3. Experimental BET Area and Pore Volume

MOF	BET Area (m^2/g)		Pore Volume, V_{pore} (cc/g)	
	NU	NCNR	NU	NCNR
HKUST-1	1740	1980	0.70	0.75
NOTT-112	3490	3440	1.46	1.44
NU-125	3120	3230	1.31	1.33
rht-MOF-7	2117	1950	0.85	0.79
Cu-MOF-74	1232	1270	0.47	0.47
PCN-250	1760	1780	0.71	0.71
NU-1000	2270	2200	1.50	1.48
UiO-67	2450	2360	0.95	0.91
UiO-68-Ant	2950	3030	1.17	1.17
CYCU-3-Al	2460	2450	1.54	1.56
$Zn_2(bdc)_2(dabco)$	1970	2020	0.73	0.76
NU-1101*	-	4340	-	1.72
NU-1102*	-	3720	-	1.65
NU-1103*	-	6245	-	2.72

* The values for NU-1101, NU-1102, and NU-1103 were obtained from Gómez-Gualdrón *et. al.*[14]

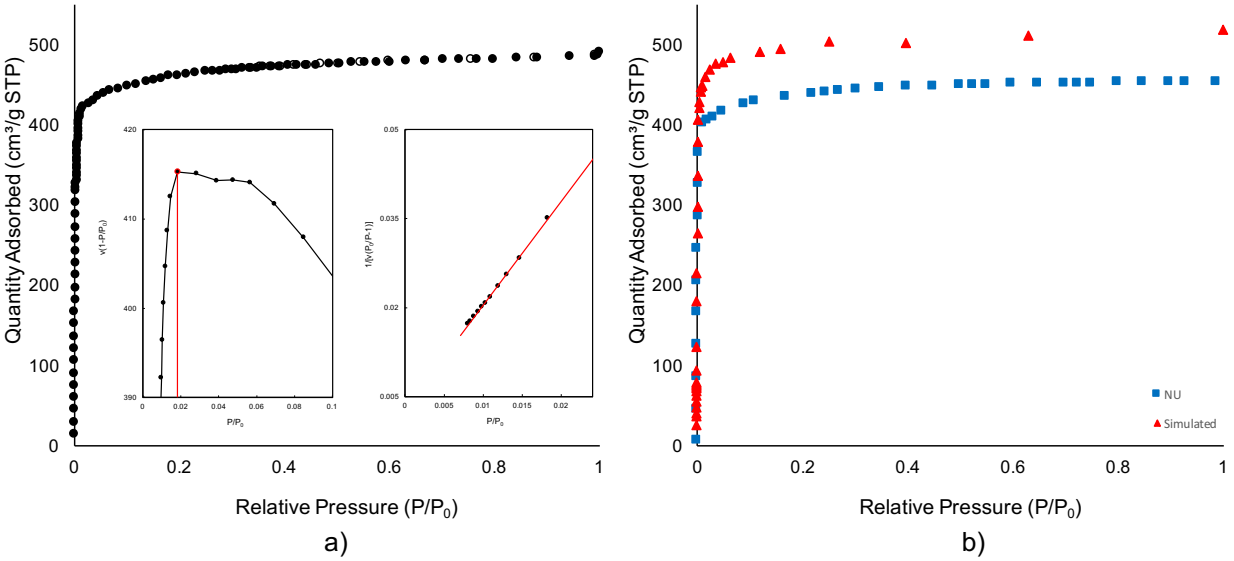

Figure S18. a) Experimental N_2 adsorption (filled points) and desorption (unfilled points) isotherms for HKUST-1 at 77 K measured at NIST. Consistency plot to determine pressure range for application of the BET fitting (inset left) and BET fitting (inset right). Plot of linear region for the BET equation and fitting (inset right). b) Experimental N_2 adsorption isotherm measured at Northwestern University (blue squares) and simulated (red triangles).

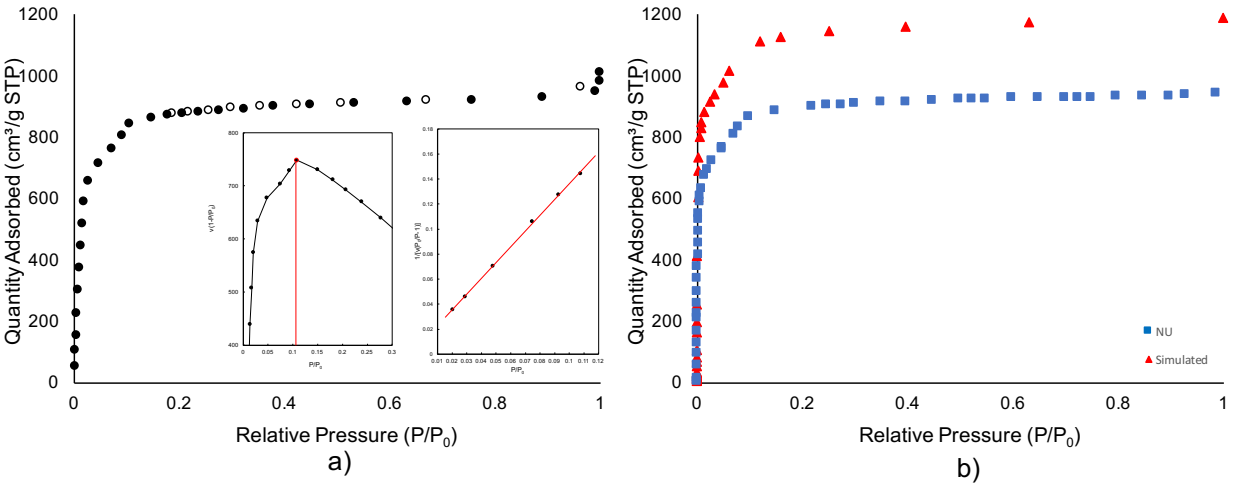

Figure S19. a) Experimental N_2 adsorption (filled points) and desorption (unfilled points) isotherms for NOTT-112 at 77 K measured at NIST. Consistency plot to determine pressure range for application of the BET fitting (inset left) and BET fitting (inset right). Plot of linear region for the BET equation and fitting (inset right). b) Experimental N_2 adsorption isotherm measured at Northwestern University (blue squares) and simulated (red triangles).

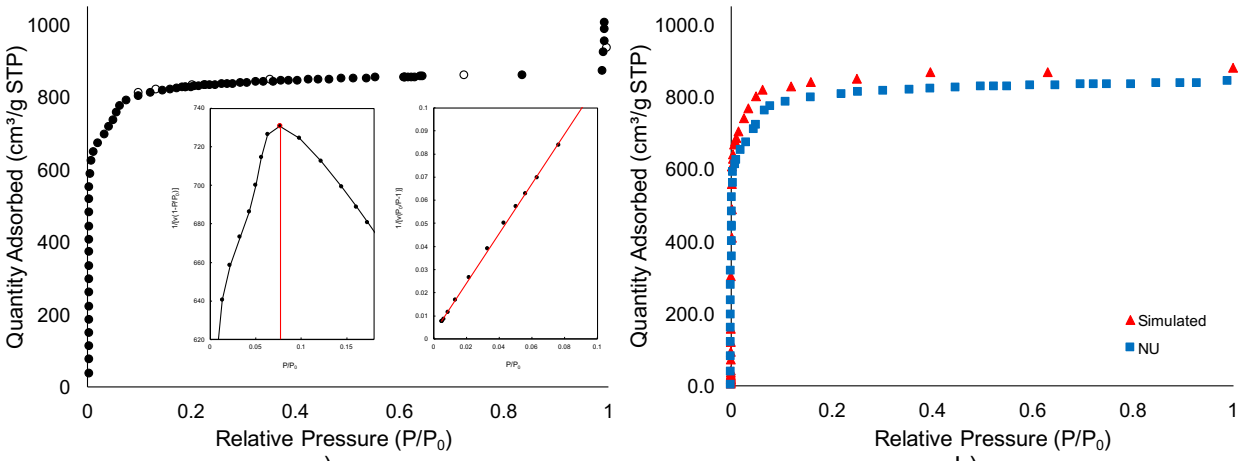

Figure S20. a) Experimental N_2 adsorption (filled points) and desorption (unfilled points) isotherms for NU-125 at 77 K measured at NIST. Consistency plot to determine pressure range for application of the BET fitting (inset left) and BET fitting (inset right). Plot of linear region for the BET equation and fitting (inset right). b) Experimental N_2 adsorption isotherm measured at Northwestern University (blue squares) and simulated (red triangles).

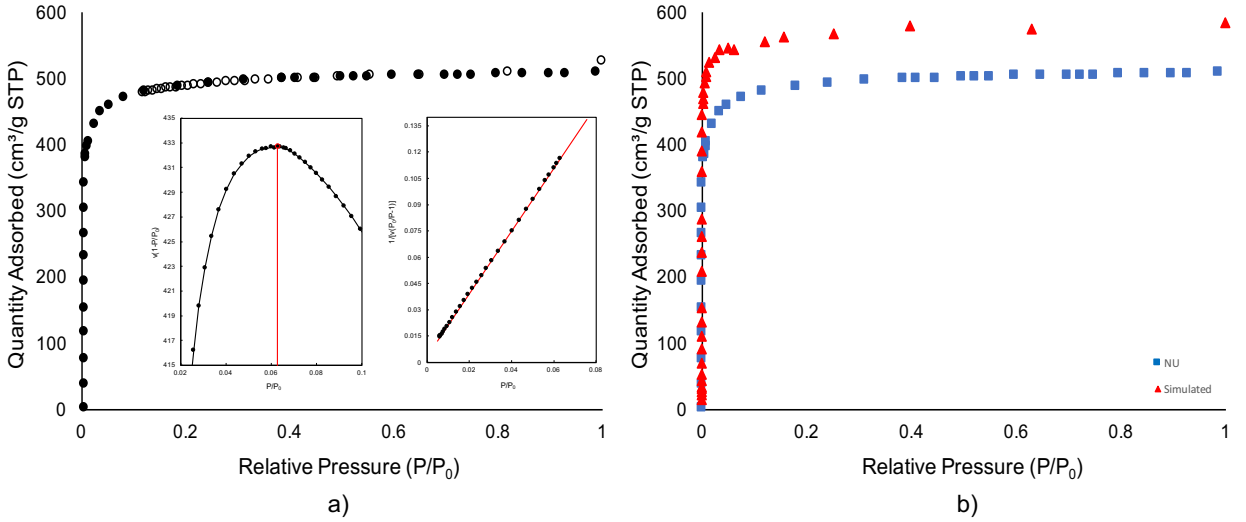

Figure S21. a) Experimental N_2 adsorption (filled points) and desorption (unfilled points) isotherms for rht-MOF-7 at 77 K measured at NIST. Consistency plot to determine pressure range for application of the BET fitting (inset left) and BET fitting (inset right). Plot of linear region for the BET equation and fitting (inset right). b) Experimental N_2 adsorption isotherm measured at Northwestern University (blue squares) and simulated (red triangles).

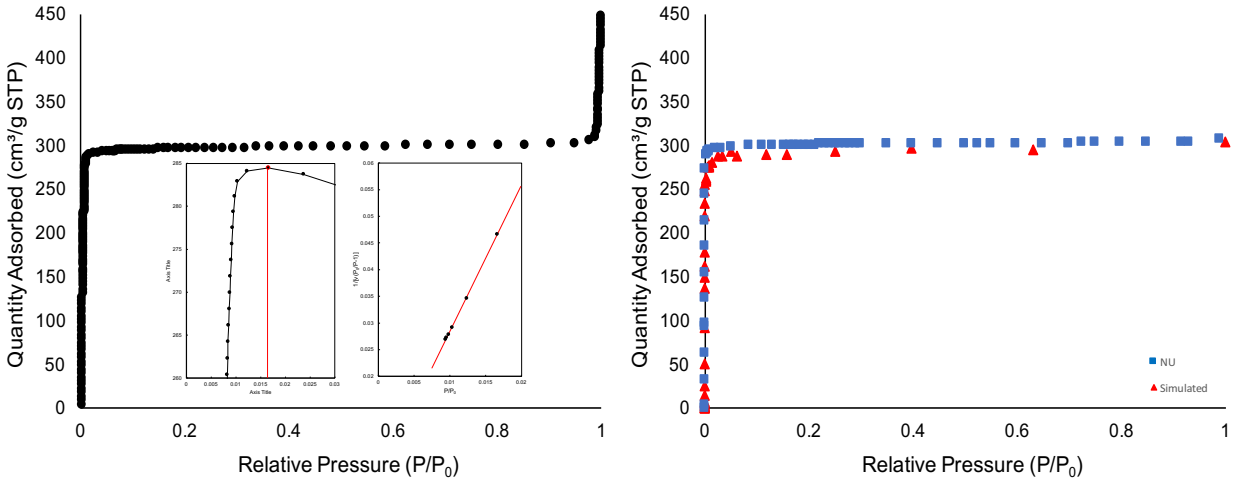

Figure S22. a) Experimental N_2 adsorption isotherm for Cu-MOF-74 at 77 K measured at NIST. Consistency plot to determine pressure range for application of the BET fitting (inset left) and BET fitting (inset right). Plot of linear region for the BET equation and fitting (inset right). b) Experimental N_2 adsorption isotherm measured at Northwestern University (blue squares) and simulated (red triangles).

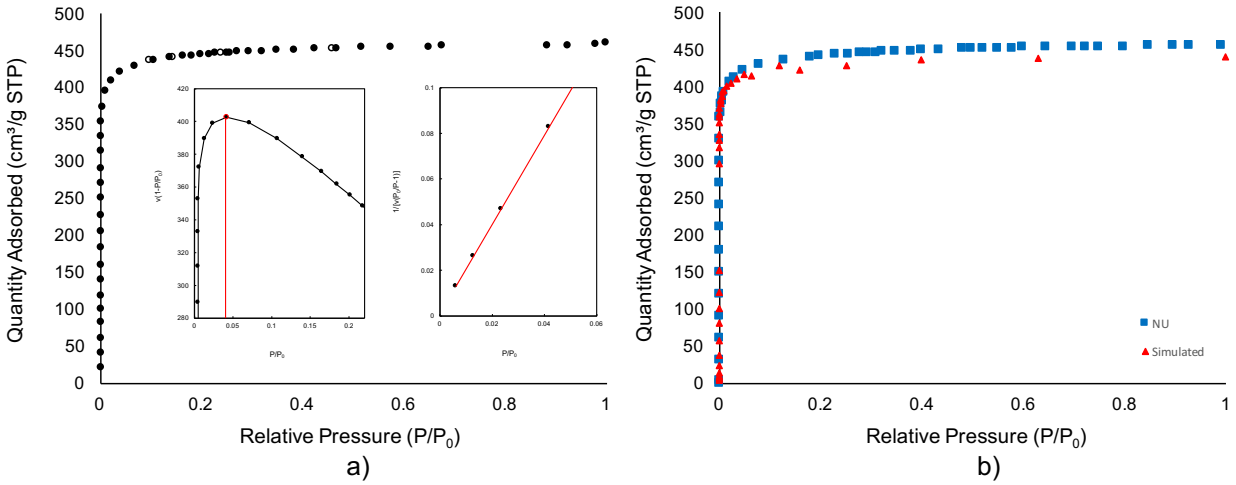

Figure S23. a) Experimental N_2 adsorption (filled points) and desorption (unfilled points) isotherms for PCN-250 at 77 K measured at NIST. Consistency plot to determine pressure range for application of the BET fitting (inset left) and BET fitting (inset right). Plot of linear region for the BET equation and fitting (inset right). b) Experimental N_2 adsorption isotherm measured at Northwestern University (blue squares) and simulated (red triangles).

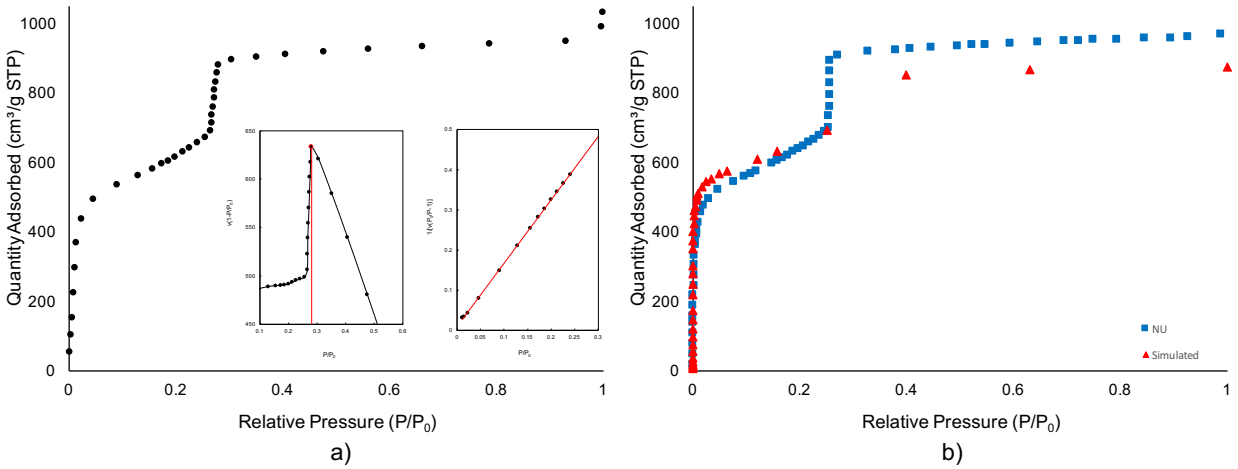

Figure S24. a) Experimental N_2 adsorption isotherm for NU-1000 at 77 K measured at NIST. Consistency plot to determine pressure range for application of the BET fitting (inset left) and BET fitting (inset right). Plot of linear region for the BET equation and fitting (inset right). b) Experimental N_2 adsorption isotherm measured at Northwestern University (blue squares) and simulated (red triangles).

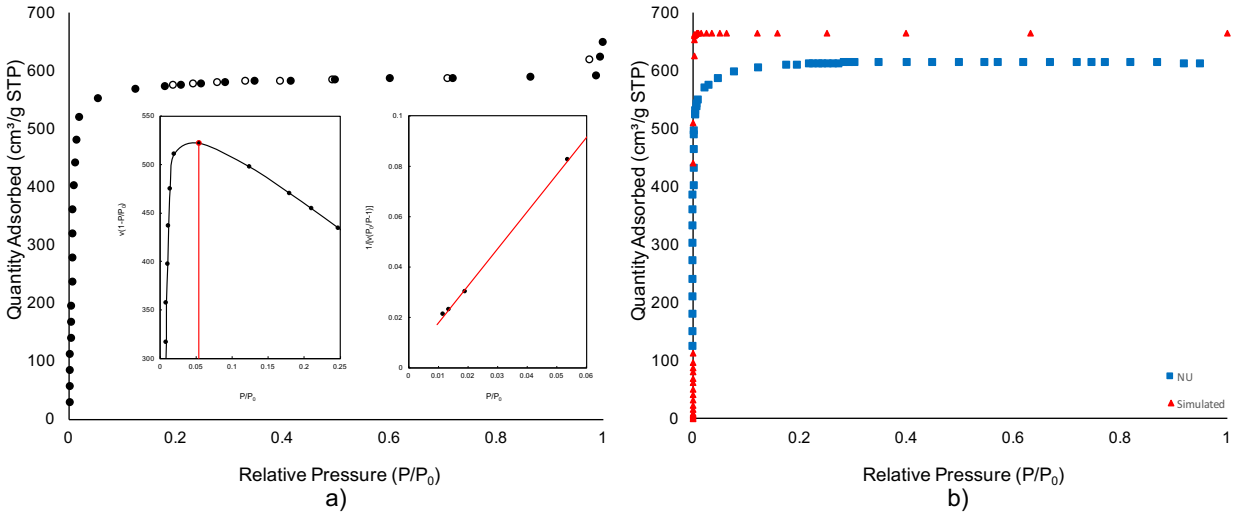

Figure S25. a) Experimental N_2 adsorption (filled points) and desorption (unfilled points) isotherms for UiO-67 at 77 K measured at NIST. Consistency plot to determine pressure range for application of the BET fitting (inset left) and BET fitting (inset right). Plot of linear region for the BET equation and fitting (inset right). b) Experimental N_2 adsorption isotherm measured at Northwestern University (blue squares) and simulated (red triangles).

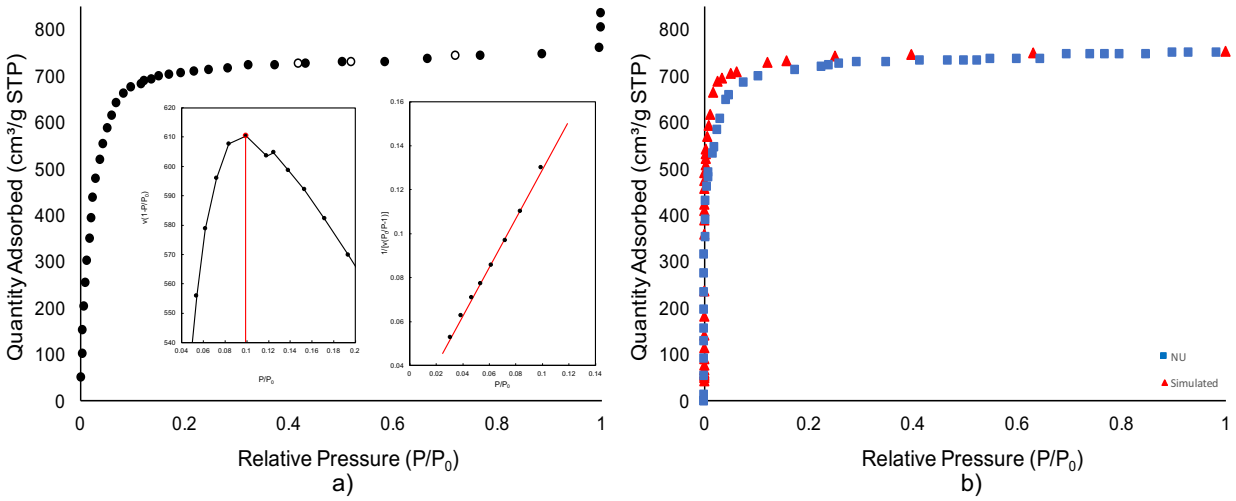

Figure S26. a) Experimental N_2 adsorption (filled points) and desorption (unfilled points) isotherms for UiO-68-Ant at 77 K measured at NIST. Consistency plot to determine pressure range for application of the BET fitting (inset left) and BET fitting (inset right). Plot of linear region for the BET equation and fitting (inset right). b) Experimental N_2 adsorption isotherm measured at Northwestern University (blue squares) and simulated (red triangles).

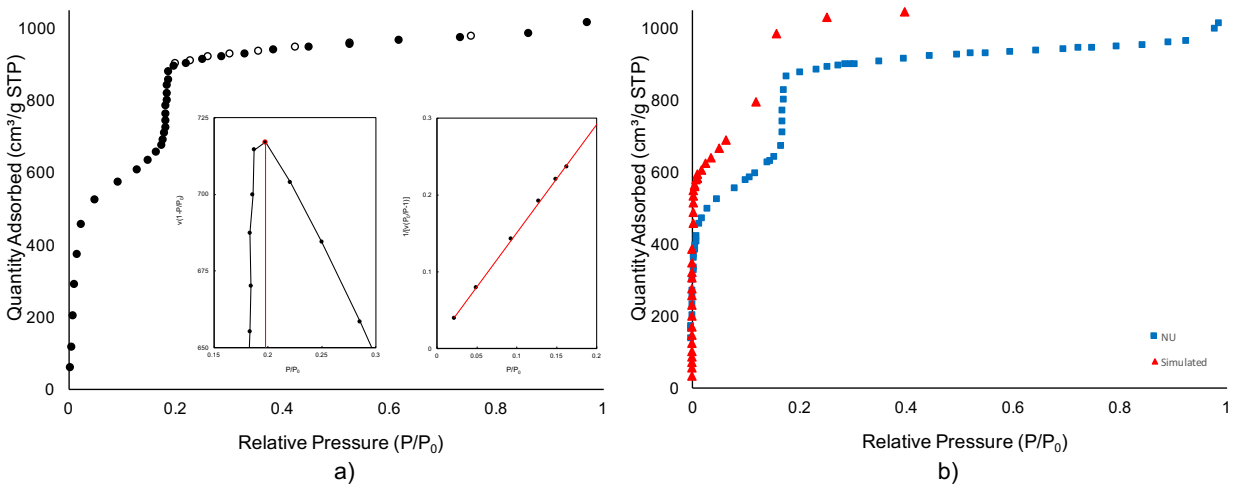

Figure S27. a) Experimental N_2 adsorption (filled points) and desorption (unfilled points) isotherms for CYCU-3-Al at 77 K measured at NIST. Consistency plot to determine pressure range for application of the BET fitting (inset left) and BET fitting (inset right). Plot of linear region for the BET equation and fitting (inset right). b) Experimental N_2 adsorption isotherm measured at Northwestern University (blue squares) and simulated (red triangles).

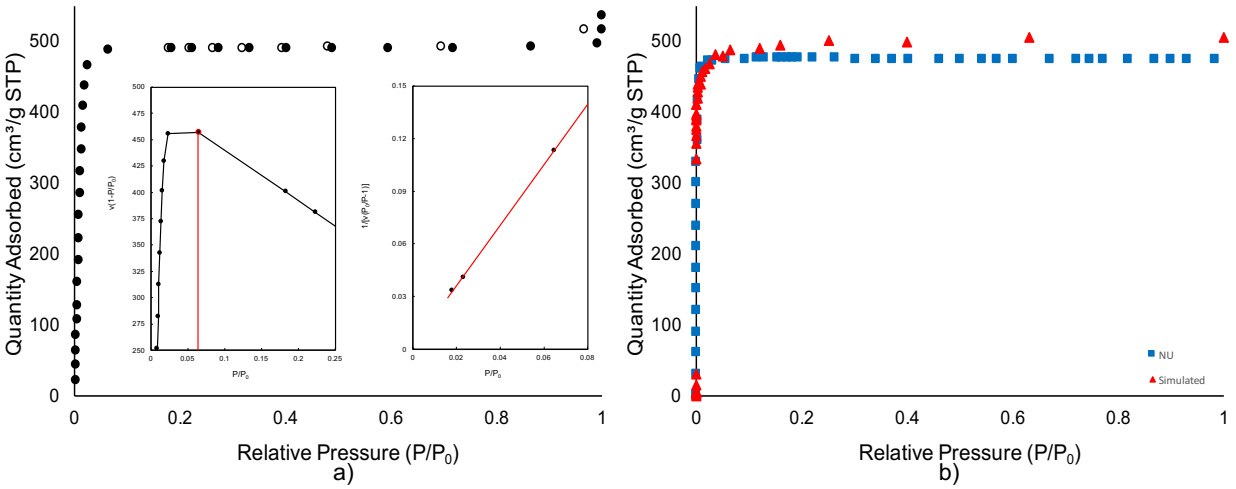

Figure S28. a) Experimental N_2 adsorption (filled points) and desorption (unfilled points) isotherms for $Zn_2(bdc)_2(dabco)$ at 77 K measured at NIST. Consistency plot to determine pressure range for application of the BET fitting (inset left) and BET fitting (inset right). Plot of linear region for the BET equation and fitting (inset right). b) Experimental N_2 adsorption isotherm measured at Northwestern University (blue squares) and simulated (red triangles).

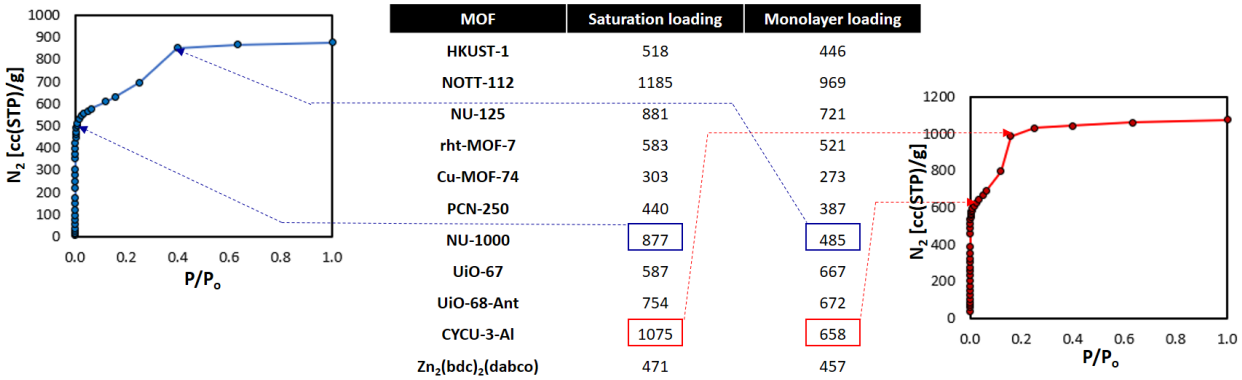

MOF	Saturation loading	Monolayer loading
HKUST-1	518	446
NOTT-112	1185	969
NU-125	881	721
rht-MOF-7	583	521
Cu-MOF-74	303	273
PCN-250	440	387
NU-1000	877	485
UiO-67	587	667
UiO-68-Ant	754	672
CYCU-3-Al	1075	658
$Zn_2(bdc)_2(dabco)$	471	457

Figure S29. Saturation loading and monolayer loadings (as calculated from BET theory) from simulated nitrogen isotherms. For NU-1000 and CYCU-3-Al the large differences between saturation and monolayer loadings is due to the large final step in the isotherm corresponding to “pore filling” of their large mesoporous channels.

Section S7. Excess and Total Hydrogen Uptakes and Isotherms

For this study excess uptake is defined as the absolute amount of gas in the MOF's pores minus the amount that is in the pores in the absence of gas while total it the total amount of adsorbate in the pores. Zhou *et. al.* provides a more detailed explanation for these concepts.[1]

Table S4. Total H_2 Uptake at 77, 160 and 296 K

MOF	Uptake 77 K 5 bar (mmol/g)	Uptake 77 K 100 bar (mmol/g)	Uptake 160 K 5 bar (mmol/g)	Uptake 160 K 100 bar (mmol/g)	Uptake 296 K 5 bar (mmol/g)	Uptake 296 K 100 bar (mmol/g)
HKUST-1	18.32	28.04	2.23	25.81	0.36	6.08
NOTT-112	21.51	47.86	2.54	45.32	0.47	8.83
NU-125	24.11	44.67	2.62	42.05	0.51	8.16
rht-MOF-7	16.71	25.68	2.13	23.55	0.34	5.72
Cu-MOF-74	11.36	16.26	1.51	14.75	0.22	3.78
PCN-250	19.58	28.35	2.43	25.92	0.34	5.75
NU-1000	17.46	43.38	2.115	41.27	0.51	8.67
UiO-67	16.69	31.14	1.85	29.29	0.33	5.74
UiO-68-Ant	19.81	41	2.34	38.66	0.38	7.31
CYCU-3-Al	17.42	44.92	1.90	43.02	0.49	8.91
$Zn_2(bdc)_2(dabco)$	17.93	25.72	1.65	24.07	0.31	5.29

Table S5. Calculated deliverable capacity of the MOFs discussed

MOF	ΔH_2@100 bar/77 K → 5 bar/77 K		ΔH_2@100 bar/77 K → 5 bar/160 K		H_2 total adsorption at 296 K	
	wt%	g/L	wt%	g/L	wt%	g/L
HKUST-1	2.5	22	5.4	48	1.2	10.8
NOTT-112	7.3	33	11.7	52	1.8	7.9
NU-125	4.9	28	9.1	53	1.6	9.5
rht-MOF-7	2.6	21	6.2	49	1.2	9.1
Cu-MOF-74	1.1	15	3.1	41	0.8	10.1
PCN-250	2.0	18	5.5	49	1.2	10.4
NU-1000	4.5	26	8.4	48	1.7	10.0
UiO-67	3.4	23	6.7	46	1.2	8.0
UiO-68-Ant	3.6	22	7.9	48	1.5	8.9
CYCU-3-Al	4.9	24	9.9	47	1.8	8.6
$Zn_2(bdc)_2(dabco)$	0.9	8	4.6	41	1.1	9.3
NU-1101*	5.9	33	9.8	51		
NU-1102*	7.7	34	11.3	52		
NU-1103*	11.9	40	14.4	51		

* The values for NU-1101, NU-1102, and NU-1103 were obtained from Gómez-Gualdrón *et. al.*[14]

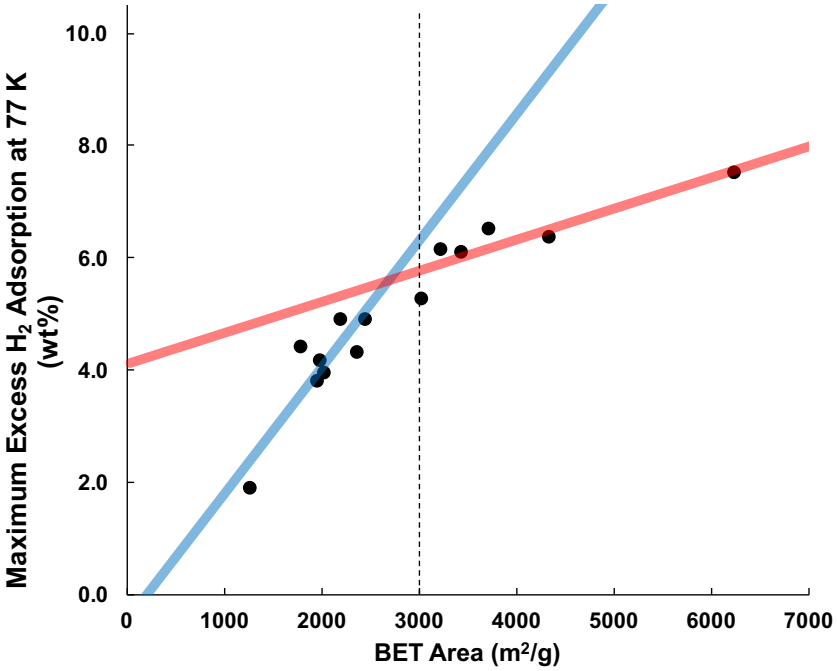

Figure S30. Excess H_2 adsorption at 77 K against BET area where a trend corresponding to 2 wt% per 1000 m^2/g (blue) can be observed before 3000 m^2/g and a trend corresponding to 0.5 wt% per 1000 m^2/g is observed after 3000 m^2/g

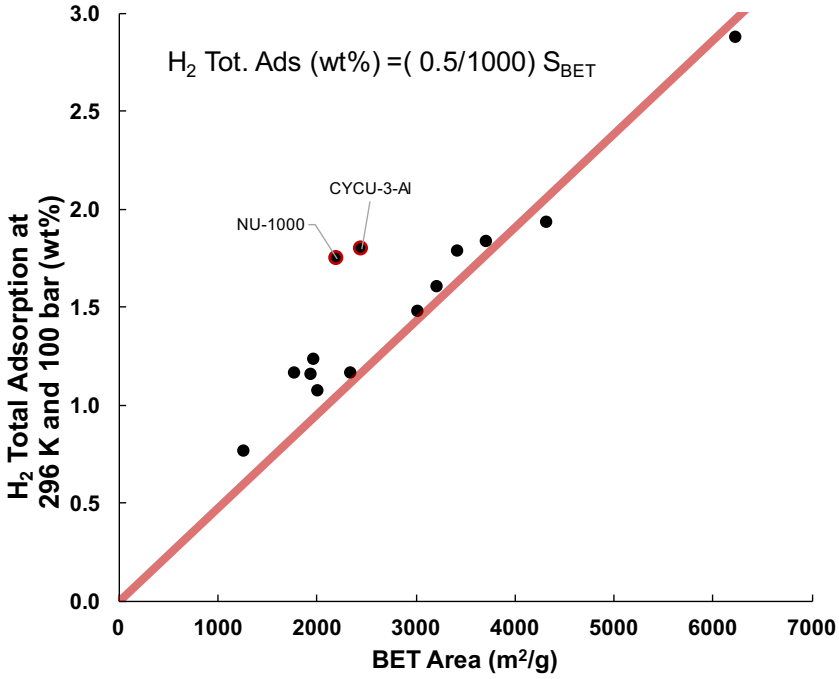

Figure S31. Excess H_2 adsorption at 296 K against BET area where a trend corresponding to 0.5 wt% per 1000 m^2/g can be observed

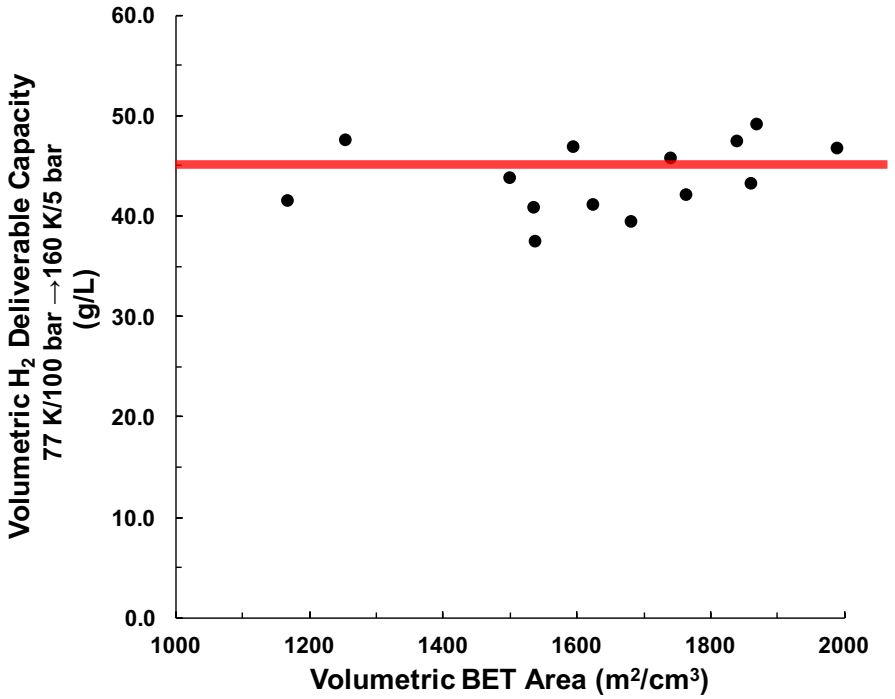

Figure S32. Volumetric H_2 deliverable capacity against volumetric BET Area. Deliverable capacity is approximately constant at 45 ± 5 g/L

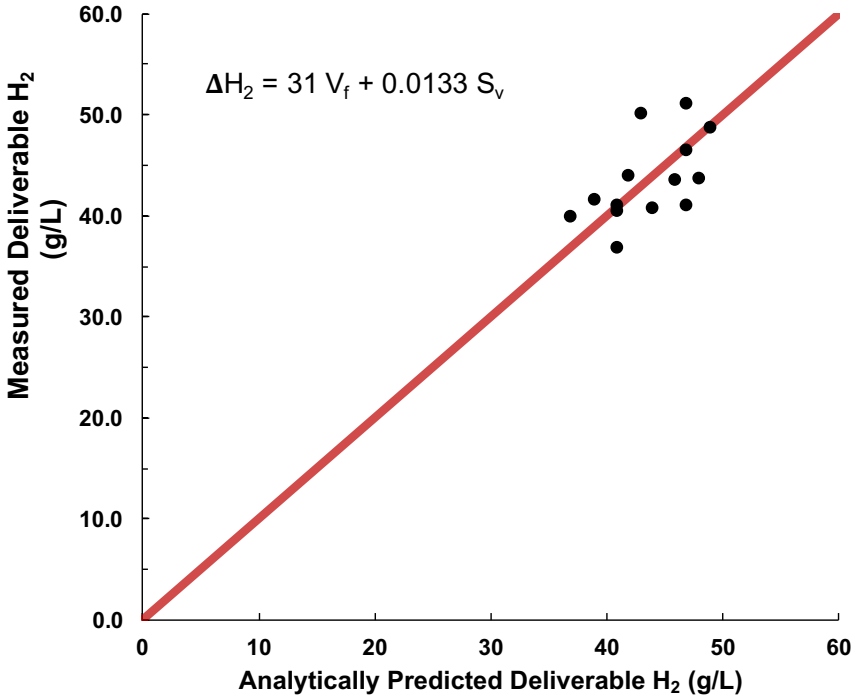

Figure S33. Measured deliverable H_2 against the predicted deliverable H_2 where 31 is the density in g/L of H_2 at 77K/bar, and 0.0133 was a fitted proportionality constant between vol. SA and the H_2 sticking to the walls.

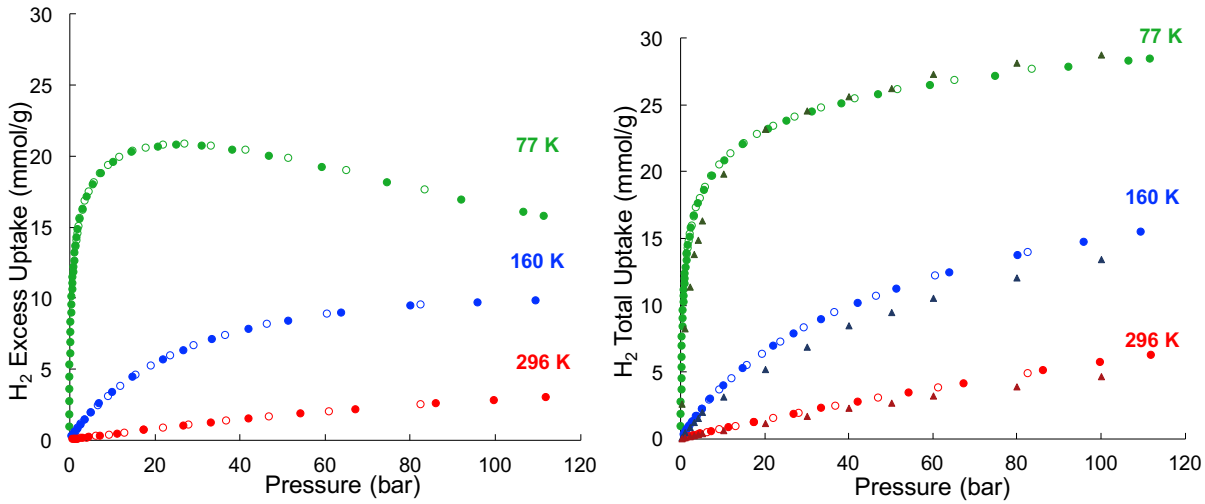

Figure S34. Excess (left) and total (right) hydrogen adsorption (filled points) and desorption (unfilled points) isotherms at 77 (green), 160 (blue) and 296 K (black) as well as simulated isotherms (filled triangles) for HKUST-1.

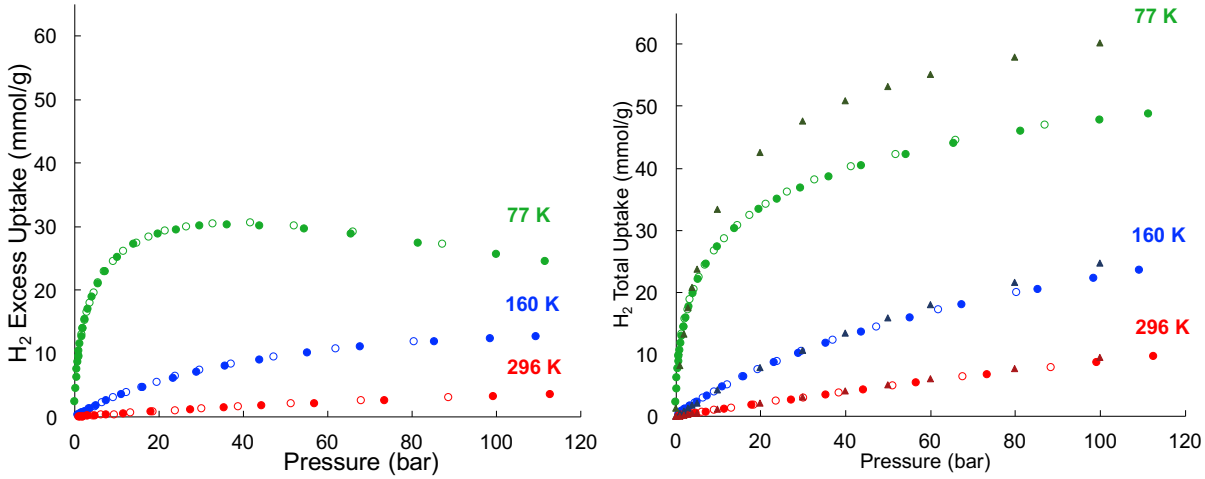

Figure S35. Excess (left) and total (right) hydrogen adsorption (filled points) and desorption (unfilled points) isotherms at 77 (green), 160 (blue) and 296 K (black) as well as simulated isotherms (filled triangles) for NOTT-112.

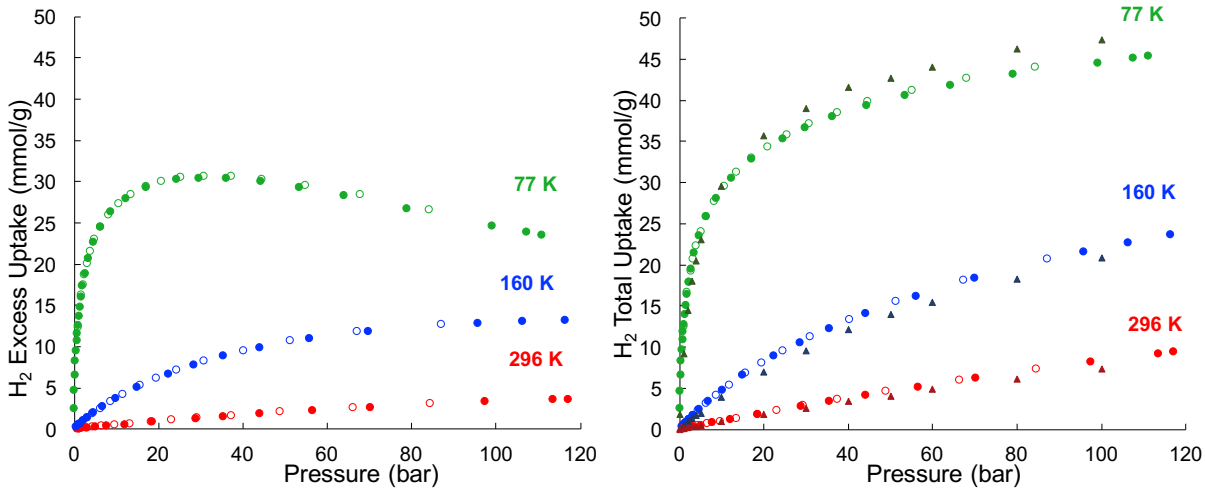

Figure S36. Excess (left) and total (right) hydrogen adsorption (filled points) and desorption (unfilled points) isotherms at 77 (green), 160 (blue) and 296 K (black) as well as simulated isotherms (filled triangles) for NU-125.

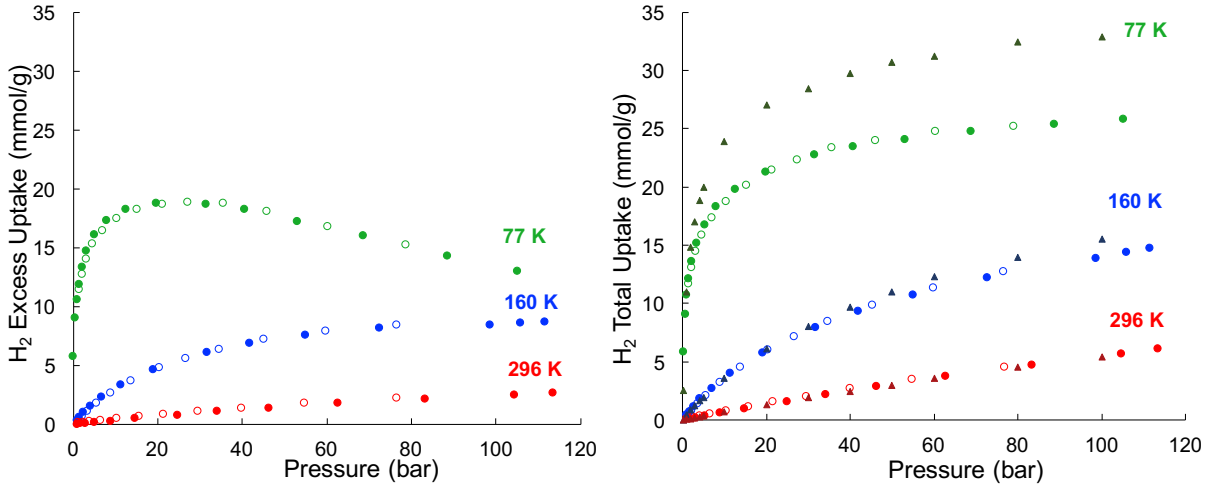

Figure S37. Excess (left) and total (right) hydrogen adsorption (filled points) and desorption (unfilled points) isotherms at 77 (green), 160 (blue) and 296 K (black) as well as simulated isotherms (filled triangles) for rht-MOF-7.

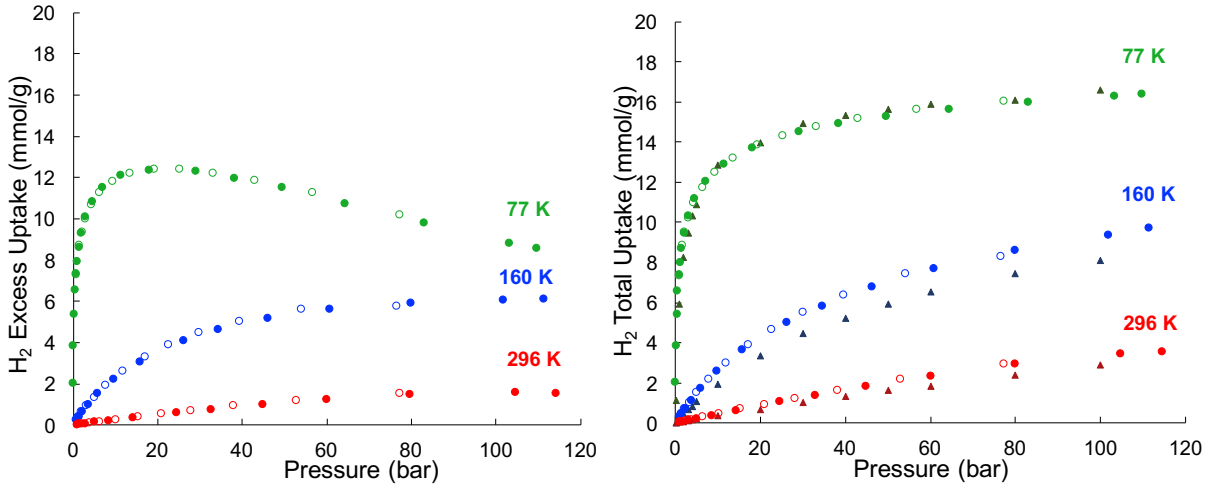

Figure S38. Excess (left) and total (right) hydrogen adsorption (filled points) and desorption (unfilled points) isotherms at 77 (green), 160 (blue) and 296 K (black) as well as simulated isotherms (filled triangles) for Cu-MOF-74.

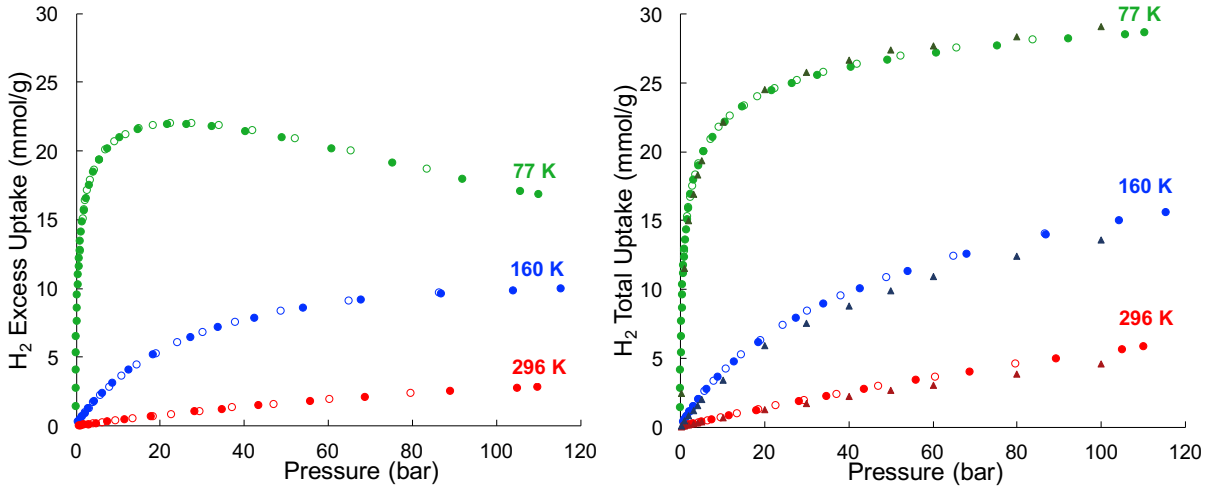

Figure S39. Excess (left) and total (right) hydrogen adsorption (filled points) and desorption (unfilled points) isotherms at 77 (green), 160 (blue) and 296 K (black) as well as simulated isotherms (filled triangles) for PCN-250

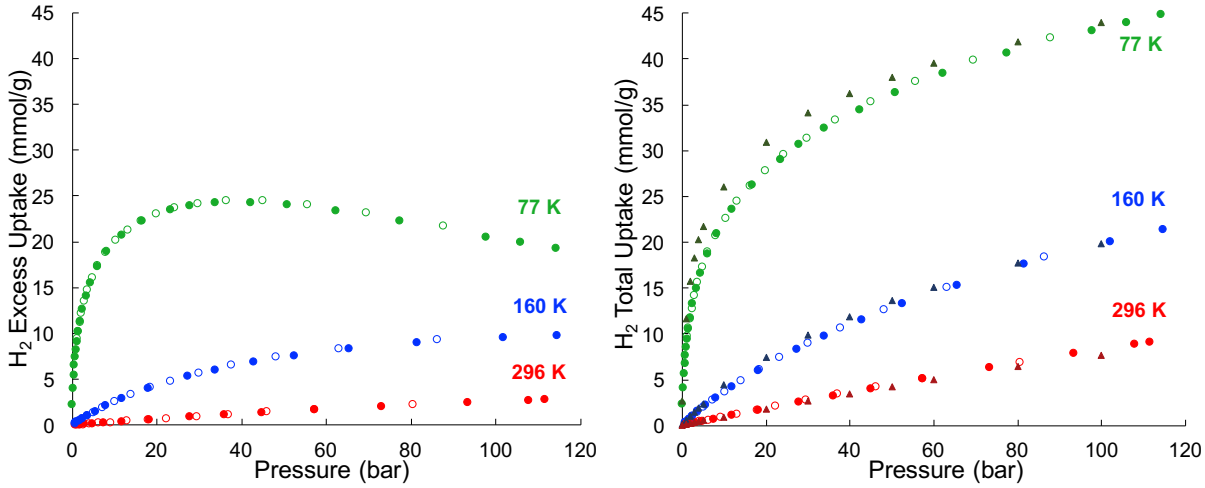

Figure S40. Excess (left) and total (right) hydrogen adsorption (filled points) and desorption (unfilled points) isotherms at 77 (green), 160 (blue) and 296 K (black) as well as simulated isotherms (filled triangles) for NU-1000.

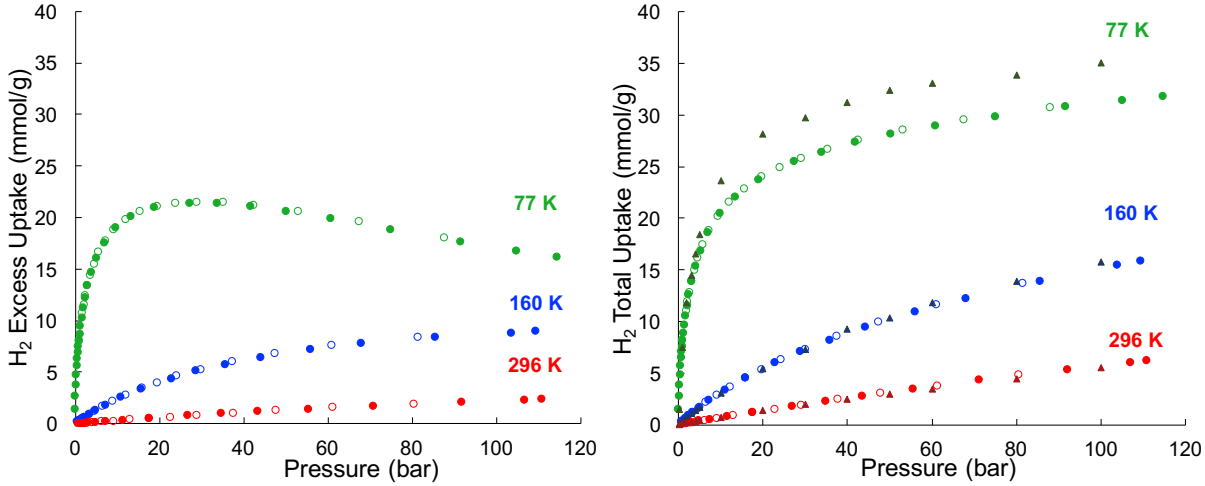

Figure S41. Excess (left) and total (right) hydrogen adsorption (filled points) and desorption (unfilled points) isotherms at 77 (green), 160 (blue) and 296 K (black) as well as simulated isotherms (filled triangles) for UiO-67.

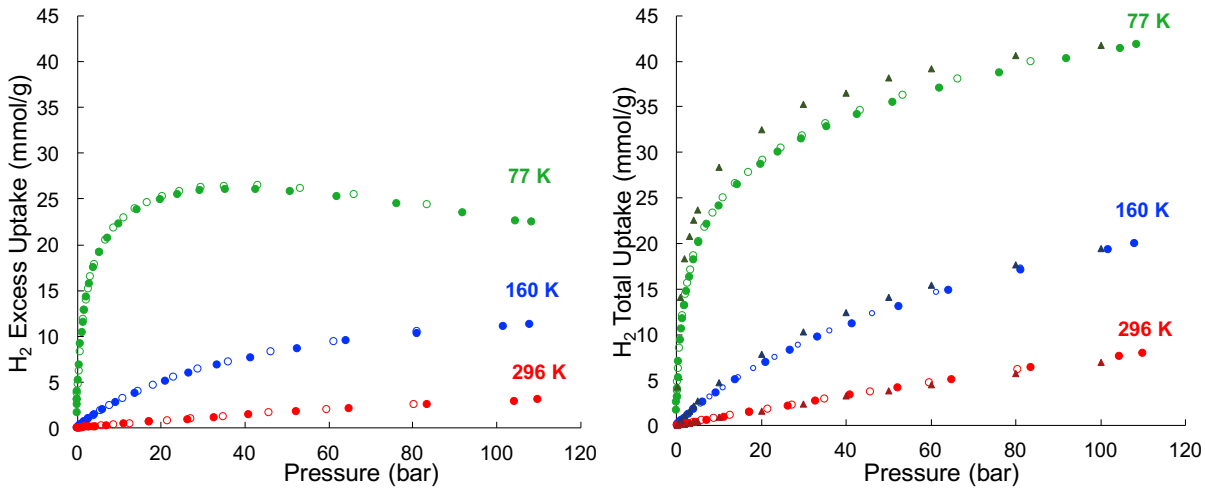

Figure S42. Excess (left) and total (right) hydrogen adsorption (filled points) and desorption (unfilled points) isotherms at 77 (green), 160 (blue) and 296 K (black) as well as simulated isotherms (filled triangles) for UiO-68-Ant.

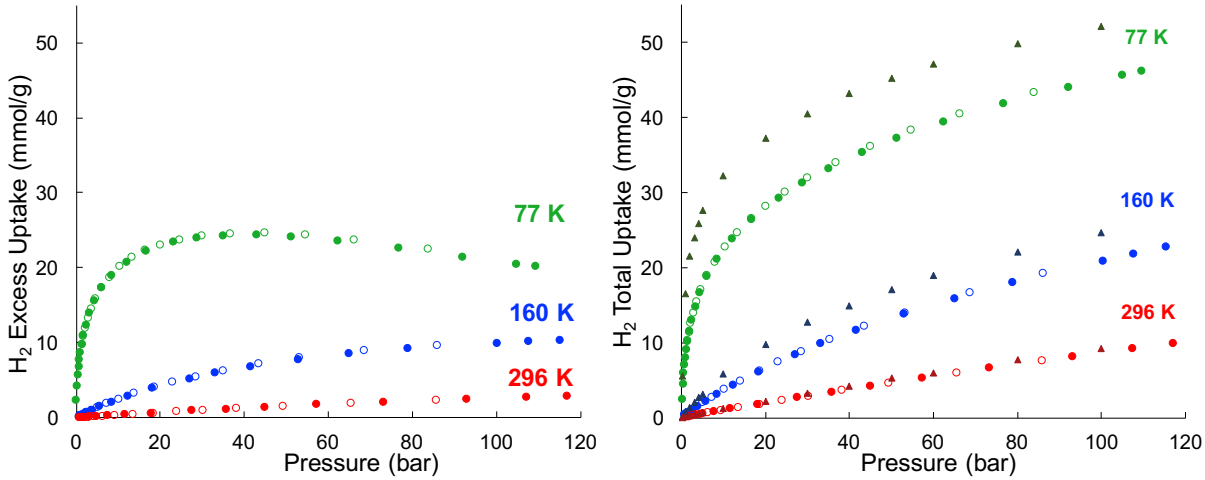

Figure S43. Excess (left) and total (right) hydrogen adsorption (filled points) and desorption (unfilled points) isotherms at 77 (green), 160 (blue) and 296 K (black) as well as simulated isotherms (filled triangles) for CYCU-3-Al.

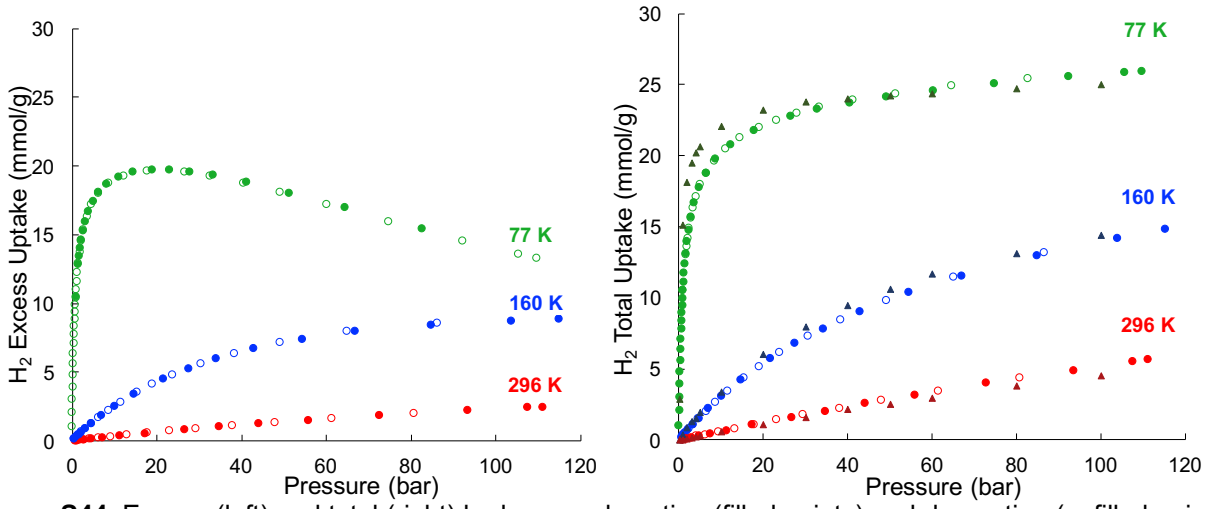

Figure S44. Excess (left) and total (right) hydrogen adsorption (filled points) and desorption (unfilled points) isotherms at 77 (green), 160 (blue) and 296 K (black) as well as simulated isotherms (filled triangles) for $Zn_2(bdc)_2(dabco)$.

Section S8. Hydrogen Isosteric Heat of Adsorption Q_{st}

Isosteric heats of adsorption (Q_{st}) were calculated from the H_2 total uptake isotherms at different temperatures. Using the cubic-spline method these temperature dependent isotherms were parameterized and then by interpolating the isotherm at a constant loading and thus obtaining Q_{st} from ln(P) versus 1/T plots. Additionally, Q_{st} was obtained by fitting the isotherms to the virial equation and then applying the Clausis-Clapeyron equation. Jagiello *et. al.* provides further details for this method.[15, 16]

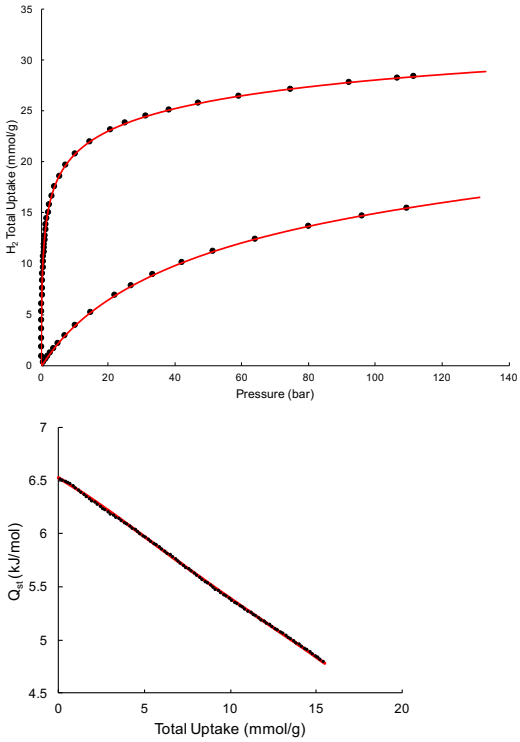

a_i	b_i
-784.62	5.6102
11.334	-0.039763
0.64936	0.0071242
-0.066476	-0.00095632
0.0034720	6.2681E-05
-0.00014164	-1.0574E-06
3.7127E-06	-1.8772E-08

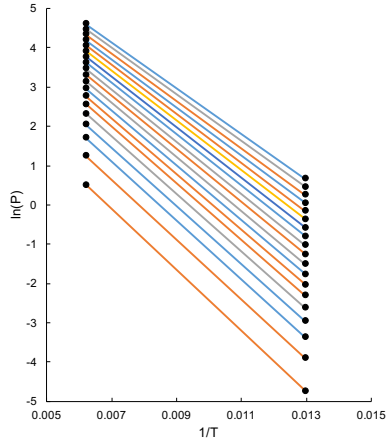

Figure S45. Hydrogen isotherms and virial fit (red line) for HKUST-1. Fit parameters (upper right), Q_{st} (lower left) and the ln(P) vs 1/T plot (lower right).

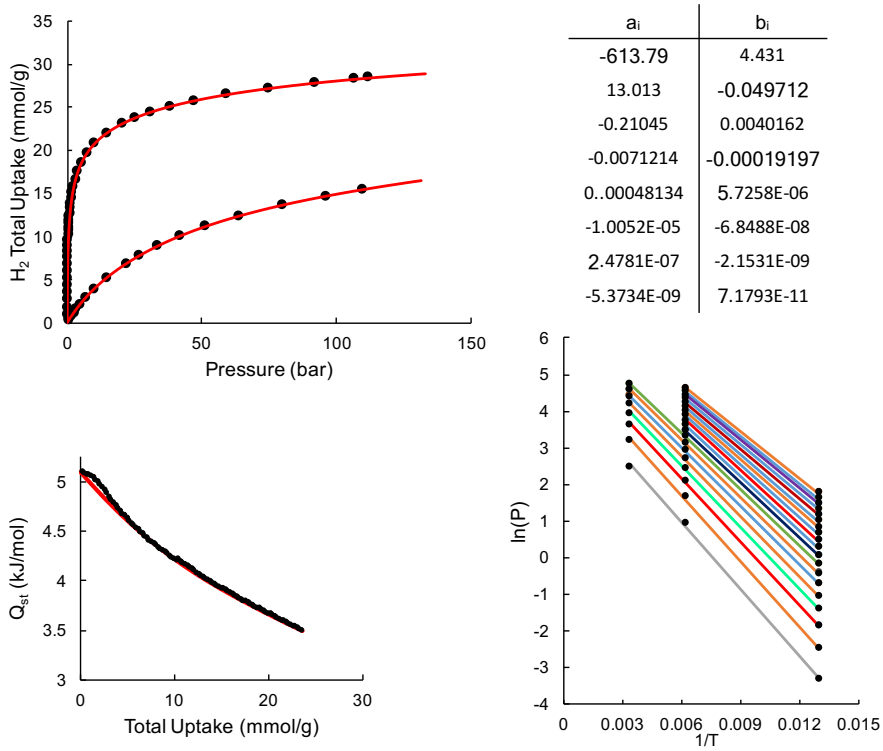

a_i	b_i
-613.79	4.431
13.013	-0.049712
-0.21045	0.0040162
-0.0071214	-0.00019197
0..00048134	5.7258E-06
-1.0052E-05	-6.8488E-08
2.4781E-07	-2.1531E-09
-5.3734E-09	7.1793E-11

Figure S46. Hydrogen isotherms and virial fit (red line) for NOTT-112. Fit parameters (upper right), Q_{st} (lower left) and the ln(P) vs 1/T plot (lower right).

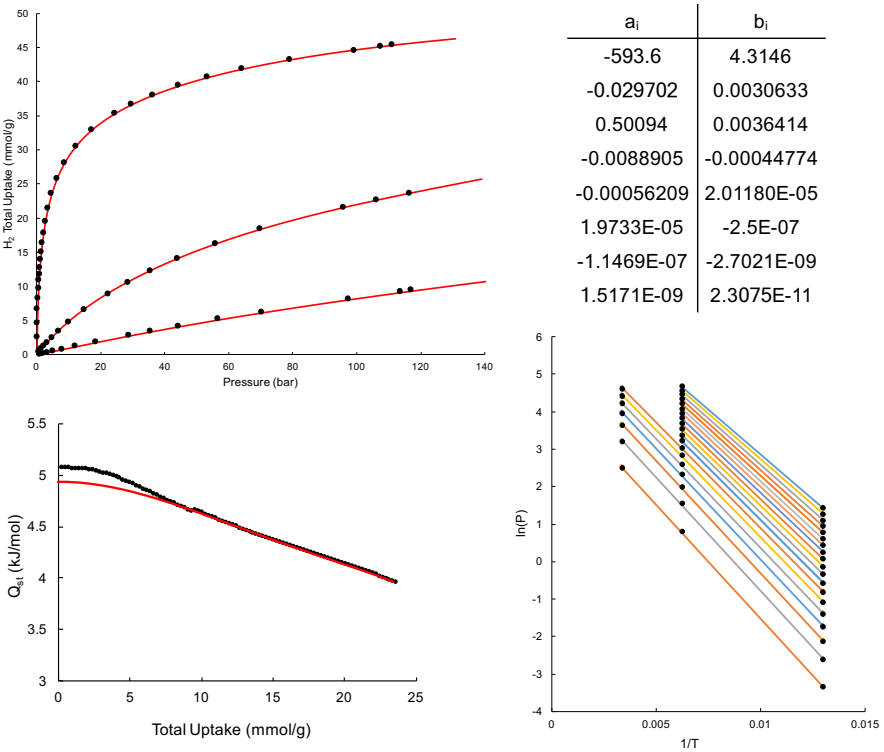

a_i	b_i
-593.6	4.3146
-0.029702	0.0030633
0.50094	0.0036414
-0.0088905	-0.00044774
-0.00056209	2.01180E-05
1.9733E-05	-2.5E-07
-1.1469E-07	-2.7021E-09
1.5171E-09	2.3075E-11

Figure S47. Hydrogen isotherms and virial fit (red line) for NU-125. Fit parameters (upper right), Q_{st} (lower left) and the ln(P) vs 1/T plot (lower right).

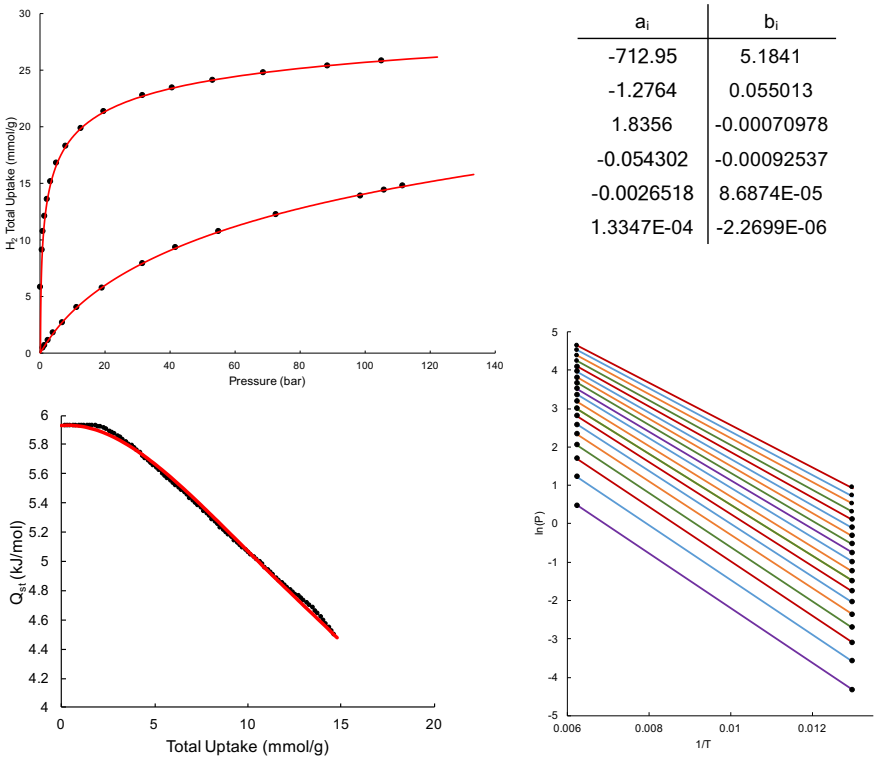

a_i	b_i
-712.95	5.1841
-1.2764	0.055013
1.8356	-0.00070978
-0.054302	-0.00092537
-0.0026518	8.6874E-05
1.3347E-04	-2.2699E-06

Figure S48. Hydrogen isotherms and virial fit (red line) for rht-MOF-7. Fit parameters (upper right), Q_{st} (lower left) and the ln(P) vs 1/T plot (lower right).

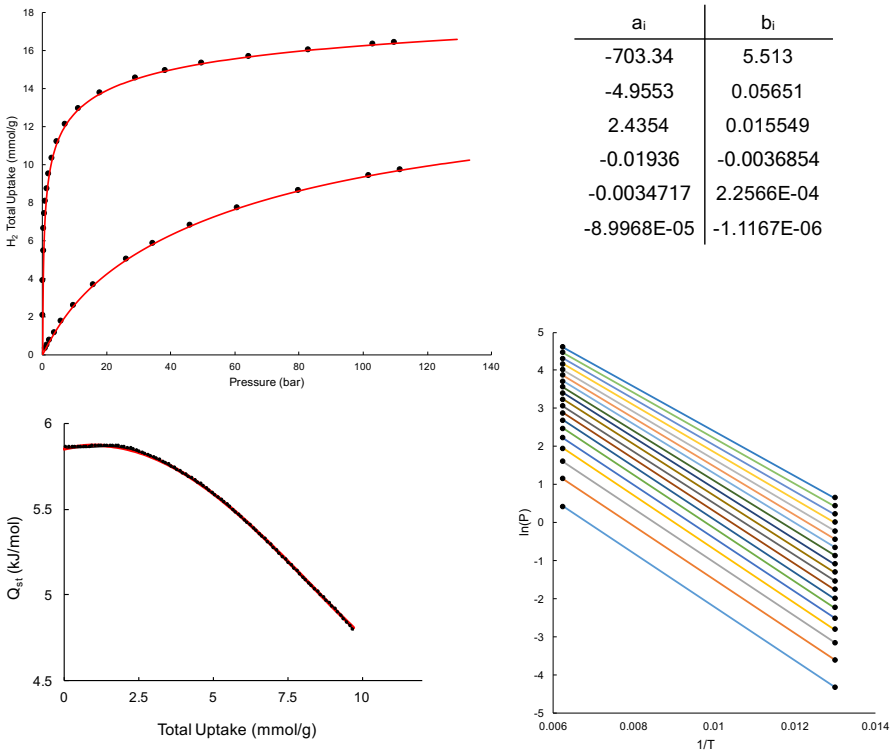

a_i	b_i
-703.34	5.513
-4.9553	0.05651
2.4354	0.015549
-0.01936	-0.0036854
-0.0034717	2.2566E-04
-8.9968E-05	-1.1167E-06

Figure S49. Hydrogen isotherms and virial fit (red line) for Cu-MOF-74. Fit parameters (upper right), Q_{st} (lower left) and the ln(P) vs 1/T plot (lower right).

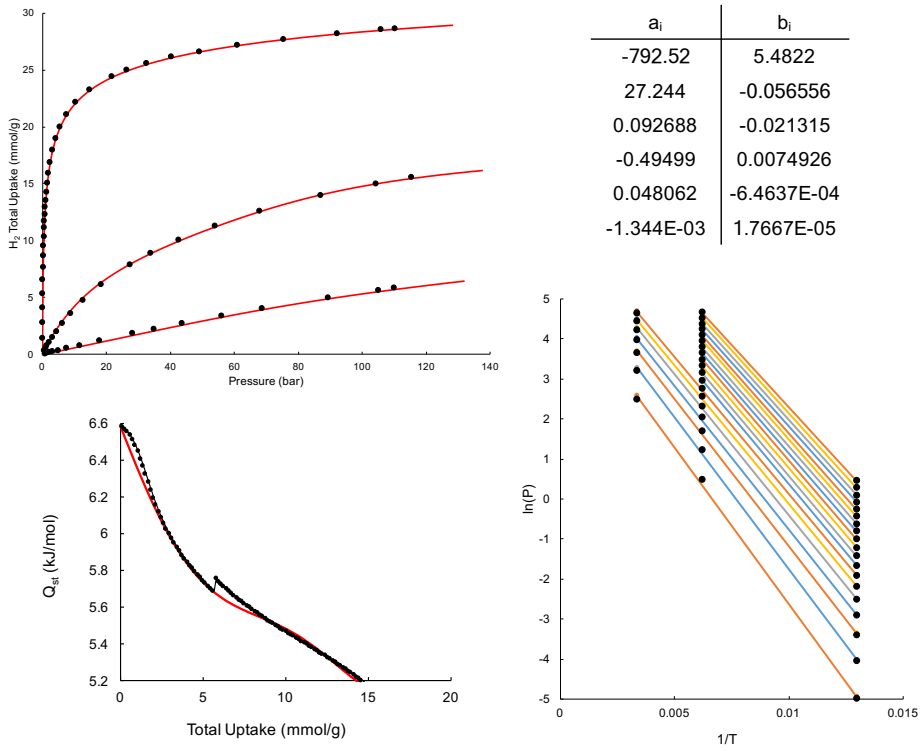

a_i	b_i
-792.52	5.4822
27.244	-0.056556
0.092688	-0.021315
-0.49499	0.0074926
0.048062	-6.4637E-04
-1.344E-03	1.7667E-05

Figure S50. Hydrogen isotherms and virial fit (red line) for PCN-250. Fit parameters (upper right), Q_{st} (lower left) and the ln(P) vs 1/T plot (lower right).

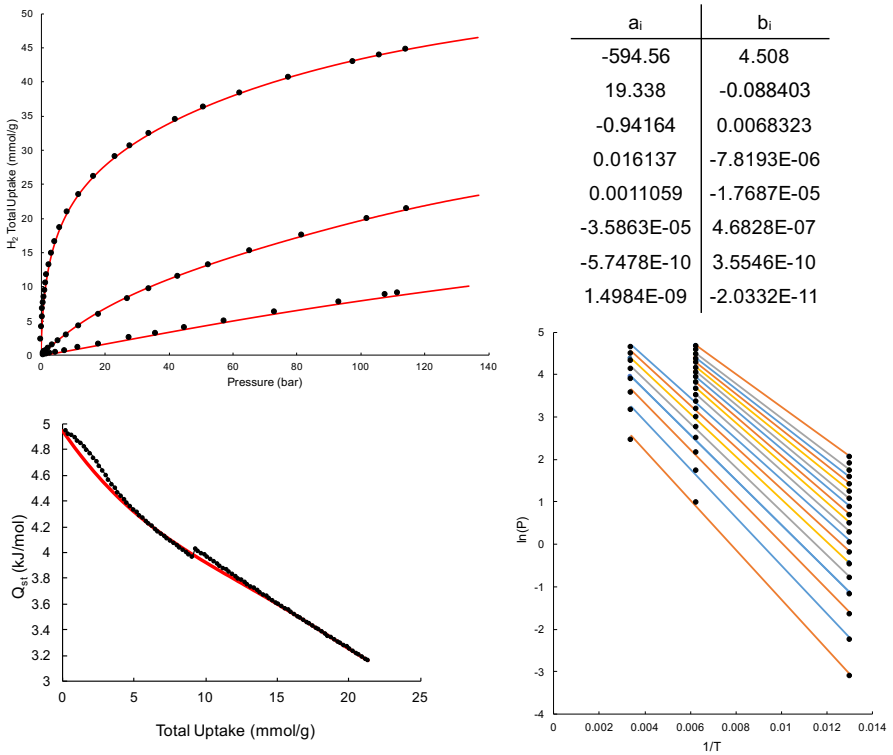

a_i	b_i
-594.56	4.508
19.338	-0.088403
-0.94164	0.0068323
0.016137	-7.8193E-06
0.0011059	-1.7687E-05
-3.5863E-05	4.6828E-07
-5.7478E-10	3.5546E-10
1.4984E-09	-2.0332E-11

Figure S51. Hydrogen isotherms and virial fit (red line) for NU-1000. Fit parameters (upper right), Q_{st} (lower left) and the ln(P) vs 1/T plot (lower right).

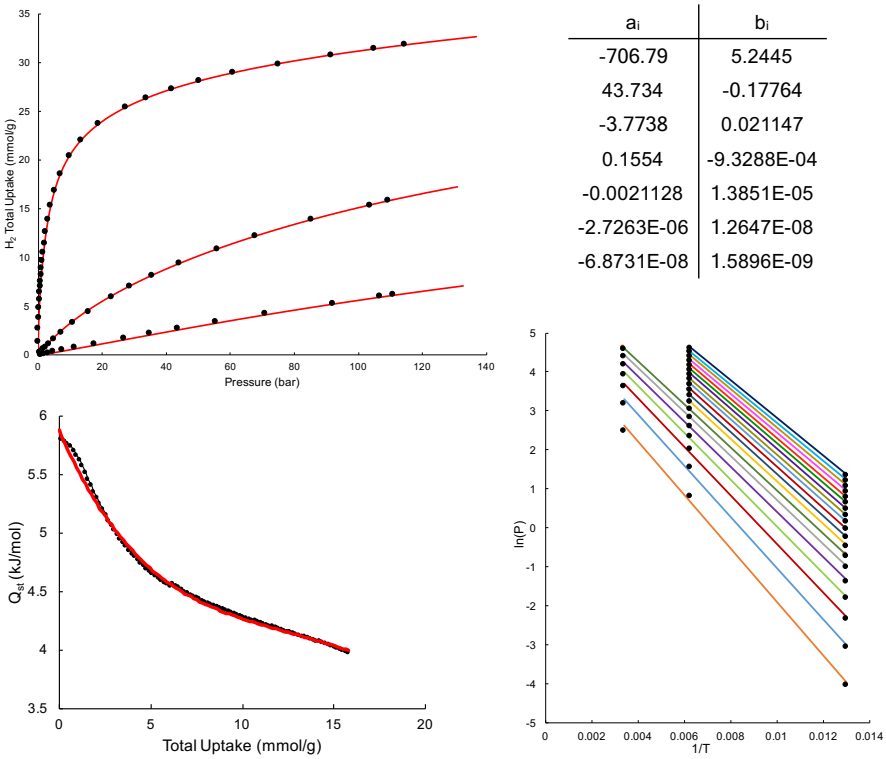

a_i	b_i
-706.79	5.2445
43.734	-0.17764
-3.7738	0.021147
0.1554	-9.3288E-04
-0.0021128	1.3851E-05
-2.7263E-06	1.2647E-08
-6.8731E-08	1.5896E-09

Figure S52. Hydrogen isotherms and virial fit (red line) for UiO-67. Fit parameters (upper right), Q_{st} (lower left) and the ln(P) vs 1/T plot (lower right).

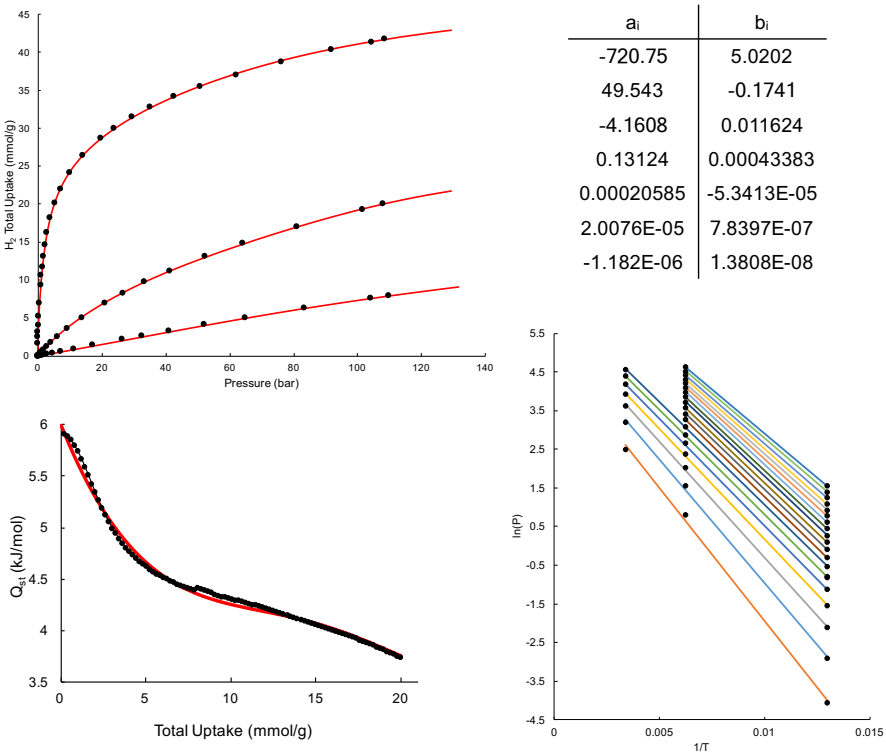

a_i	b_i
-720.75	5.0202
49.543	-0.1741
-4.1608	0.011624
0.13124	0.00043383
0.00020585	-5.3413E-05
2.0076E-05	7.8397E-07
-1.182E-06	1.3808E-08

Figure S53. Hydrogen isotherms and virial fit (red line) for UiO-68-Ant. Fit parameters (upper right), Q_{st} (lower left) and the ln(P) vs 1/T plot (lower right).

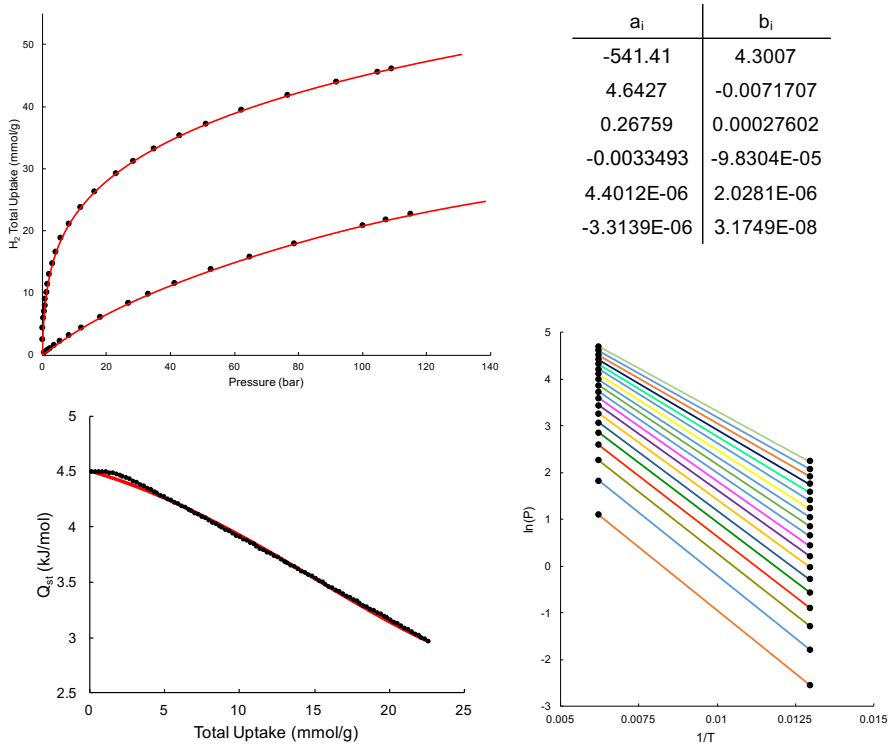

a_i	b_i
-541.41	4.3007
4.6427	-0.0071707
0.26759	0.00027602
-0.0033493	-9.8304E-05
4.4012E-06	2.0281E-06
-3.3139E-06	3.1749E-08

Figure S54. Hydrogen isotherms and virial fit (red line) for CYCU-3-Al. Fit parameters (upper right), Q_{st} (lower left) and the lnP-1/T plot (lower right).

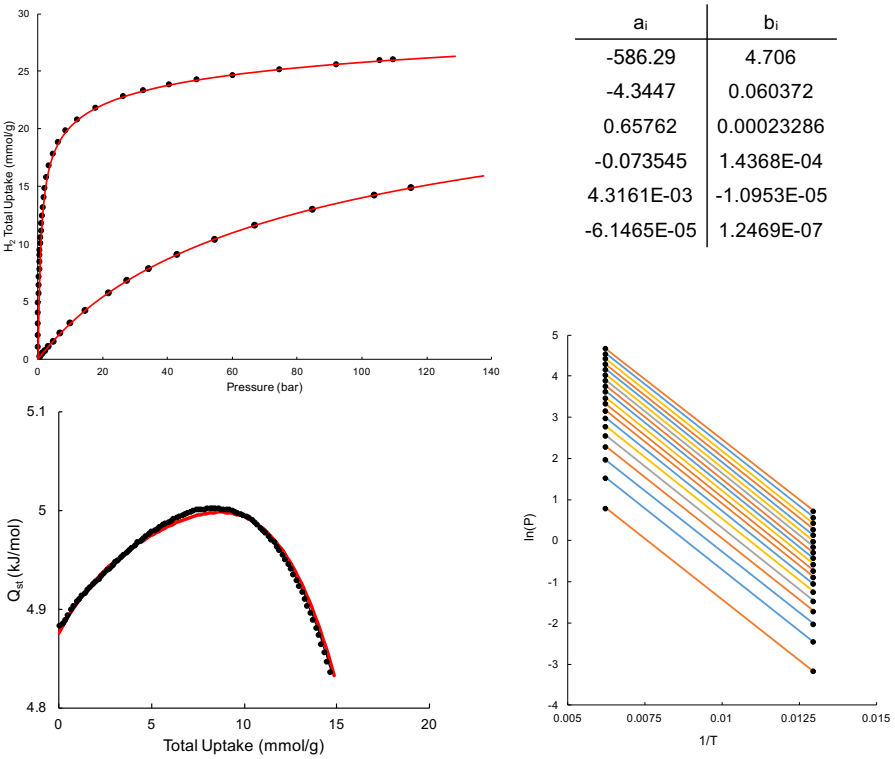

a_i	b_i
-586.29	4.706
-4.3447	0.060372
0.65762	0.00023286
-0.073545	1.4368E-04
4.3161E-03	-1.0953E-05
-6.1465E-05	1.2469E-07

Figure S55. Hydrogen isotherms and virial fit (red line) for $Zn_2(bdc)_2(dabco)$. Fit parameters (upper right), Q_{st} (lower left) and the ln(P) vs 1/T plot (lower right).

Section S9. References Cited

1. Zhou, W.; Wu, H.; Hartman, M. R.; Yildirim, T. *J. Phys. Chem. C* **2007**, 111, 16131.
2. Wilmer, C. E.; Farha, O. K.; Yildirim, T.; Eryazici, I.; Krungleviciute, V.; Sarjeant, A. A.; Snurr, R. Q.; Hupp, J. T. *Energy Environ. Sci.* **2013**, 6, 1158.
3. Feng, D.; Wang, K.; Wei, Z.; Chen, Y.-P.; Simon, C. M.; Arvapally, R. K.; Martin, R. L.; Bosch, M.; Liu, T.-F.; Fordham, S.; Yuan, D.; Omary, M. A.; Haranczyk, M.; Smit, B.; Zhou, H.-C. *Nat. Commun.* **2014**, 5, 5723.
4. Dybtsev, D. N.; Chun, H.; Kim, K. *Angew. Chem. Int. Ed.* **2004**, 43, 5033.
5. Peng, Y.; Krungleviciute, V.; Eryazici, I.; Hupp, J. T.; Farha, O. K.; Yildirim, T. *J. Am. Chem. Soc.* **2013**, 135, 11887.
6. Mondloch, J. E.; Bury, W.; Fairen-Jimenez, D.; Kwon, S.; DeMarco, E. J.; Weston, M. H.; Sarjeant, A. A.; Nguyen, S. T.; Stair, P. C.; Snurr, R. Q.; Farha, O. K.; Hupp, J. T. *J. Am. Chem. Soc.* **2013**, 135, 10294.
7. Wang, T. C.; Vermeulen, N. A.; Kim, I. S.; Martinson, A. B. F.; Stoddart, J. F.; Hupp, J. T.; Farha, O. K. *Nat. Protoc.* **2016**, 11, 149.
8. Liu, Y.; Klet, R. C.; Hupp, J. T.; Farha, O. *Chem. Commun.* **2016**, 52, 7806.
9. Wang, C.; Volotskova, O.; Lu, K.; Ahmad, M.; Sun, C.; Xing, L.; Lin, W. *J. Am. Chem. Soc.* **2014**, 136, 6171.
10. Lo, S.-H.; Chien, C.-H.; Lai, Y.-L.; Yang, C.-C.; Lee, J. J.; Raja, D. S.; Lin, C.-H. *J. Mater. Chem. A* **2013**, 1, 324.
11. Ma, D.; Li, B.; Zhou, X.; Zhou, Q.; Liu, K.; Zeng, G.; Li, G.; Shi, Z.; Feng, S. *Chem. Commun.* **2013**, 49, 8964.
12. Luebke, R.; Eubank, J. F.; Cairns, A. J.; Belmabkhout, Y.; Wojtas, L.; Eddaoudi, M. *Chem. Commun.* **2012**, 48, 1455.
13. Walton, K. S.; Snurr, R. Q. *J. Am. Chem. Soc.* **2007**, 129, 8552.
14. Gómez-Gualdrón, D.A.; Wang,T.C.; García-Holley,P.; Sawelewa, R. M.; Argueta, E.; Snurr, R. Q.; Hupp, J. T.; Yildirim, T.; Farha, O. K. *ACS Appl. Mater. Interfaces* **2017**, 9, 33419.
15. Jagiello, J.; Bandosz, T. J.; Putyera, K.; Schwarz, J. A. *J. Chem. Eng. Data* **1995**, 40, 1288.
16. Jagiello, J.; Bandosz, T. J.; Schwarz, J. A. *Langmuir* **1996**, 12, 2837.